Title

The midbody ring scaffolds the abscission machinery in the absence of midbody microtubules

Journal

Journal of Cell Biology, 203(3)

ISSN

0021-9525

Authors

Green, Rebecca A
Mayers, Jonathan R
Wang, Shaohe
et al.

Publication Date

2013-11-11

DOI

10.1083/jcb.201306036

Peer reviewed

The midbody ring scaffolds the abscission machinery in the absence of midbody microtubules

Rebecca A. Green,[1] Jonathan R. Mayers,[2] Shaohe Wang,[1] Lindsay Lewellyn,[3] Arshad Desai,[1] Anjon Audhya,[2] and Karen Oegema[1]

[1]Department of Cellular and Molecular Medicine, Ludwig Institute for Cancer Research, University of California, San Diego, La Jolla, CA 92093
[2]Department of Biomolecular Chemistry, School of Medicine and Public Health, University of Wisconsin–Madison, Madison, WI 53705
[3]Department of Biological Sciences, Butler University, Indianapolis, IN 46208

Abscission completes cytokinesis to form the two daughter cells. Although abscission could be organized from the inside out by the microtubule-based midbody or from the outside in by the contractile ring–derived midbody ring, it is assumed that midbody microtubules scaffold the abscission machinery. In this paper, we assess the contribution of midbody microtubules versus the midbody ring in the *Caenorhabditis elegans* embryo. We show that abscission occurs in two stages. First, the cytoplasm in the daughter cells becomes isolated, coincident with formation of the intercellular bridge; proper progression through this stage required the septins (a midbody ring component) but not the membrane-remodeling endosomal sorting complex required for transport (ESCRT) machinery. Second, the midbody and midbody ring are released into a specific daughter cell during the subsequent cell division; this stage required the septins and the ESCRT machinery. Surprisingly, midbody microtubules were dispensable for both stages. These results delineate distinct steps during abscission and highlight the central role of the midbody ring, rather than midbody microtubules, in their execution.

Introduction

Cytokinesis can be partitioned into two phases: (1) contractile ring constriction, which changes cell shape, and (2) abscission, which isolates the cytoplasm in the daughter cells and alters membrane topology to form two physically distinct cells. Contractile ring constriction is orchestrated by an array of antiparallel microtubule bundles called the central spindle and a cortical contractile ring that forms around the cell equator. As constriction nears completion, the central spindle and contractile ring mature to form the midbody and the midbody ring, which direct abscission (Fededa and Gerlich, 2012; Green et al., 2012; Agromayor and Martin-Serrano, 2013).

The midbody is a densely packed antiparallel microtubule array that sits in the center of the intercellular bridge (Glotzer, 2009; Green et al., 2012). The molecular composition of the midbody includes three key components also required to form the central spindle: (1) the microtubule cross-linking protein PRC1 (Glotzer, 2009; Walczak and Shaw, 2010), (2) the centralspindlin complex, consisting of the Mklp1 kinesin and the CYK4 Rho GAP (White and Glotzer, 2012), and (3) the chromosomal passenger complex containing the Aurora B kinase (Carmena et al., 2012). Whereas PRC1 and the chromosomal passenger complex remain associated with midbody microtubules (Hu et al., 2012), centralspindlin transitions in its localization from the midbody to the midbody ring (Elia et al., 2011; Hu et al., 2012).

The midbody ring, like the midbody, retains contractile ring components, including actin filaments, Myosin II, and septin filaments, as well as Anillin and Citron kinase (Madaule et al., 1998; Gai et al., 2011; Hu et al., 2012; Kechad et al., 2012). The septins bind directly to the plasma membrane and are recruited to the contractile ring by Anillin (D'Avino, 2009; Piekny and Maddox, 2010; Oh and Bi, 2011; Mostowy and Cossart, 2012). In *Drosophila melanogaster* S2 cells, the Anillin N terminus, which binds actin and Myosin II, is important for midbody ring integrity, whereas the connection between the Anillin C terminus and the septins links the midbody ring to the plasma membrane (Kechad et al., 2012), a role similar to that proposed for the CYK4 C1 domain (Lekomtsev et al., 2012).

Correspondence to Karen Oegema: koegema@ucsd.edu

Abbreviations used in this paper: CCD, charge-coupled device; dsRNA, double-stranded RNA; ESCRT, endosomal sorting complex required for transport; NID, normalized intensity difference; PH, pleckstrin homology.

The Rockefeller University Press $30.00
J. Cell Biol. Vol. 203 No. 3 505–520
www.jcb.org/cgi/doi/10.1083/jcb.201306036

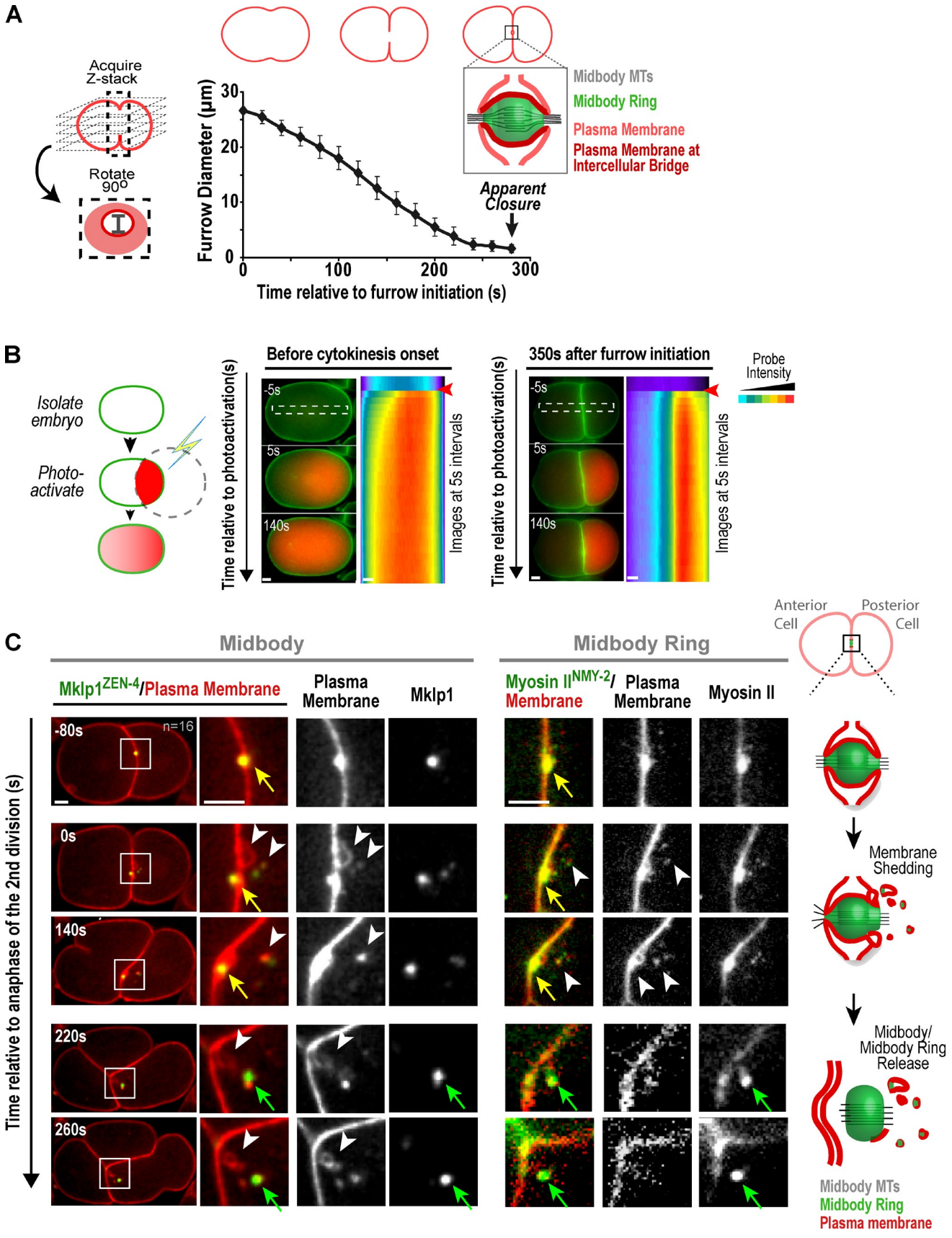

Figure 1. **Abscission occurs in two stages: cytoplasmic isolation and release of the midbody/midbody ring.** (A) Furrow diameter was measured in projections of the central region of z stacks of embryos (n = 10) expressing a GFP-tagged plasma membrane probe. (right) Graph plots mean furrow diameter versus time after furrow initiation. Arrow indicates the last time point when a hole can be detected (apparent closure). Error bars are the SDs. (top) Schematics illustrate shape changes during the first division in the *C. elegans* embryo, highlighting intercellular bridge structure. MTs, microtubules. (B, left)

Abscission could be organized from the outside in by the midbody ring or from the inside out by the midbody. Although the relative contributions of the midbody and midbody ring in scaffolding abscission have not been directly tested, the midbody is thought to serve as the platform that brings together the abscission machinery, including membrane trafficking components that narrow the intercellular bridge (Schiel and Prekeris, 2013) and the endosomal sorting complex required for transport (ESCRT) machinery, which executes the final scission event (Agromayor and Martin-Serrano, 2013; McCullough et al., 2013). In human cells, the ESCRT machinery is recruited by CEP55, which binds to centralspindlin late in cytokinesis; CEP55 binds Alix and ESCRT-I, which in turn recruit ESCRT-III proteins thought to polymerize to drive membrane scission (Fabbro et al., 2005; Zhao et al., 2006; Carlton and Martin-Serrano, 2007; Morita et al., 2007; Carlton et al., 2008; Lee et al., 2008; Bastos and Barr, 2010; Elia et al., 2011; Guizetti et al., 2011).

The point when the cytoplasm in the daughter cells becomes isolated from each other (hereafter termed cytoplasmic isolation) has been monitored by following the diffusion of fluorescent probes (Lo and Gilula, 1979; Sanger et al., 1985; Steigemann et al., 2009; Guizetti et al., 2011). In HeLa cells, cytoplasmic exchange ceases ∼60 min after the completion of furrowing, coincident with ESCRT-III–mediated scission (Steigemann et al., 2009; Guizetti et al., 2011).

Here, we analyze abscission in the early *Caenorhabditis elegans* embryo. We show that abscission occurs in two stages: cytoplasmic isolation and midbody/midbody ring release. Inhibition of the midbody ring–associated septins affects both stages, whereas the membrane-remodeling ESCRT machinery is only required for the second stage. In contrast to the idea that the midbody plays a central role in orchestrating abscission, both cytoplasmic isolation and midbody ring release occur normally in the absence of midbody microtubules. These results define distinct events during abscission and highlight the central role of the midbody ring, rather than midbody microtubules, in directing abscission.

Results

Cytoplasmic isolation occurs coincident with the completion of contractile ring constriction during the first division of the *C. elegans* embryo

To monitor contractile ring closure, we collected time-lapse 3D images of embryos expressing a GFP fusion with a pleckstrin homology (PH) domain that binds a phospholipid produced specifically on the plasma membrane (Audhya et al., 2005) and generated end-on views by rotating and projecting the data from the central portion of the embryo (Maddox et al., 2007). The last time when a hole can be detected is ∼280 s after furrow initiation, a point we refer to as apparent closure (Fig. 1 A). To determine whether cytoplasmic isolation is coincident with apparent closure, we loaded caged carboxy-Q-rhodamine–labeled 10-kD dextran into embryos expressing the GFP-tagged plasma membrane probe by injection into the syncytial gonad of adult worms (Fig. S1 B). Diffusion was monitored by imaging at 5-s intervals after photoactivating the probe on one side of the embryo with a pulse of UV light. Before cytokinesis onset, the photoactivated probe equilibrated between the two halves of the embryo with a half-time of ∼40 s; however, after apparent closure, there was no detectable equilibration (Fig. 1 B and Video 1). We conclude that the cytoplasm in the daughter cells becomes diffusionally isolated coincident with the completion of contractile ring constriction.

The midbody/midbody ring from the first cytokinesis is released after anaphase of the subsequent cell division

In vertebrate cells, cytoplasmic isolation is thought to occur simultaneously with ESCRT-mediated scission (Steigemann et al., 2009; Guizetti et al., 2011). Scission releases the midbody into one of the daughter cells, if the bridge is severed on one side, or into the extracellular space, if it is cut on both sides (Chen et al., 2013). Midbodies are released into the extracellular space during the Q cell neuroblast divisions in *C. elegans* larva (Chai et al., 2012). However, older work suggested that the midbody/midbody ring from the first embryonic division remains after the completion of furrowing, in which it serves as a cortical site that guides centrosome rotation at the two-cell stage (Hyman, 1989; Waddle et al., 1994; Keating and White, 1998).

To determine whether the midbody/midbody ring are released, we used live-cell imaging to monitor fluorescently tagged fusions with two midbody components, mCherry-Mklp1^{ZEN-4} and GFP–Aurora B^{AIR-2}, and two components of the midbody ring, Myosin II^{NMY-2}–GFP and GFP–CYK-7, a new contractile/midbody ring component that we recently identified (Green et al., 2011). Imaged embryos also expressed mCherry- or GFP-tagged fusions to label the plasma membrane. As contractile ring constriction completed, the two midbody markers were enveloped by the closing furrow and remained localized to a single tight focus embedded within the plasma membrane at the

Schematic illustrates the method for monitoring the diffusion of photoactivated dextran between the two half-cells before and after cytokinesis. Examples of probe diffusion in embryos photoactivated before cytokinesis onset (middle; *n* = 12 embryos) and after apparent closure (right; *n* = 8 embryos, example shown is 350 s after furrow initiation). Central plane images show the embryos before activation (−5 s), immediately after activation (5 s), and 140 s after activation (140 s). Kymographs were constructed by aligning strips (narrow rectangles) from images collected at 5-s intervals. Red arrow denotes the point of photoactivation. (C) Central plane fluorescence confocal images of embryos expressing a fluorescently tagged plasma membrane probe (red in merged images) along with either the midbody marker mCherry-Mklp1^{ZEN-4} (*n* = 18 embryos) or the midbody ring marker Myosin II^{NMY-2}–GFP (*n* = 14 embryos). Times are relative to anaphase of the second division (∼900 s after initiation of the first division furrow). Different embryos are shown to illustrate membrane shedding (−80 to 140–s time points) and midbody/midbody ring release (220–260-s time points). White boxes on the low magnification images mark the location of the region shown at higher magnification in the three adjacent panels. Loops and released fragments marked with the plasma membrane probe are indicated (white arrowheads). Yellow arrows denote mCherry-Mklp1^{ZEN-4}–marked or Myosin II^{NMY-2}–GFP-marked midbody remnants before release from the cell–cell junction. Green arrows mark the same components after release. Schematics illustrate events at each stage. Bars, 5 µm.

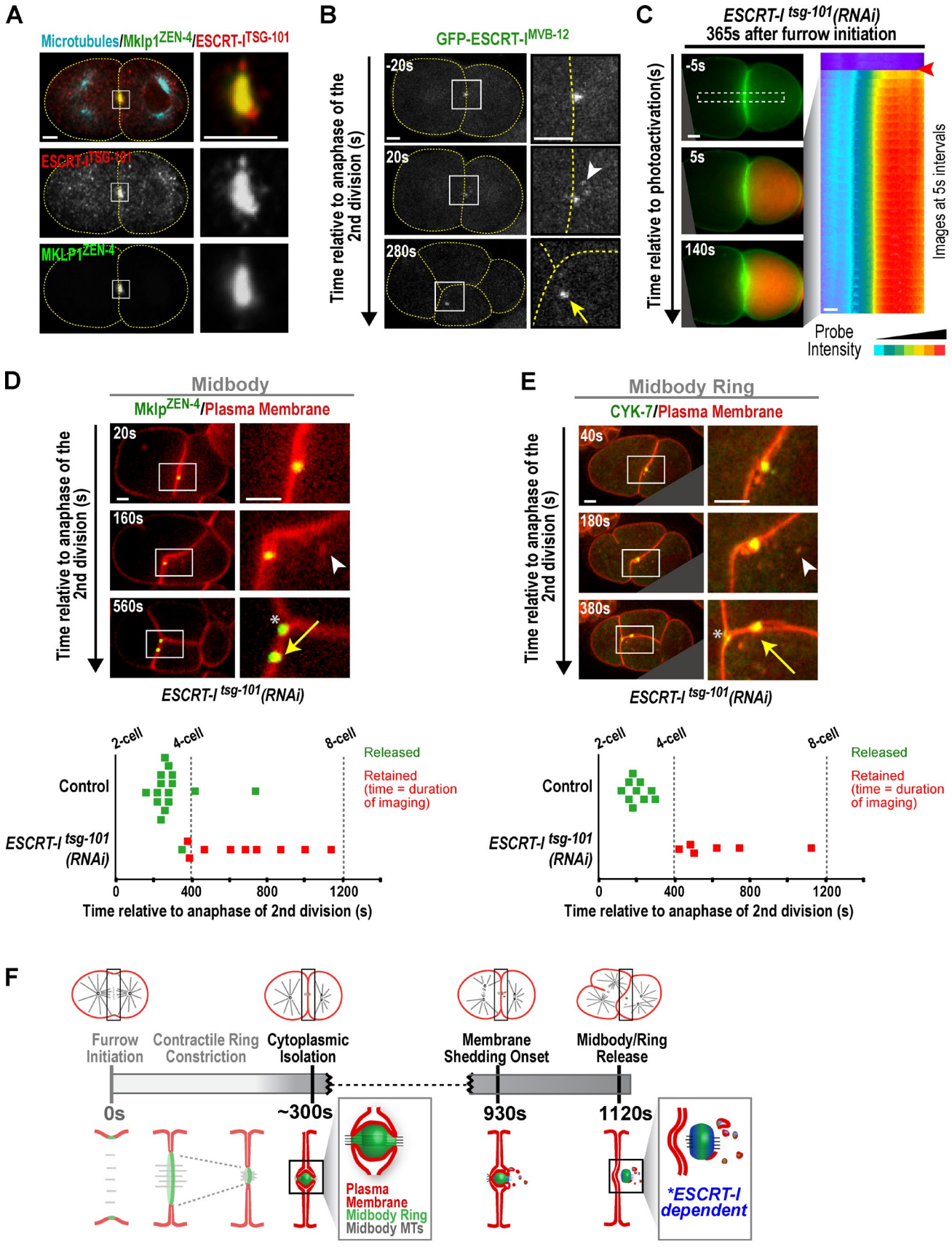

Figure 2. **The ESCRT machinery is required for midbody/midbody ring release.** (A) Deconvolved wide-field image of an embryo stained for tubulin (cyan), Mklp1^{ZEN-4}, and ESCRT-I$^{TSG-101}$ (n = 5 embryos). (B) Central plane confocal images of embryos expressing GFP–ESCRT-I^{MVB-12} (n = 6 embryos). Times are relative to anaphase of the second division. Dashed yellow lines mark the cell boundaries. The white arrowhead and yellow arrow mark the focus

cell–cell boundary, the intercellular bridge, for the next ∼12 min (Fig. 1 C, yellow arrows; and Fig. S1 C; for a comparison of the intercellular bridge in the *C. elegans* embryo and vertebrate cells see Fig. S1 A). Coincident with anaphase of the second division (in the anterior AB cell; ∼909 ± 102 s after furrow initiation), tiny pieces labeled with the plasma membrane marker were shed asymmetrically from the midbody region predominantly into the posterior cell (Fig. 1 C, white arrowheads). Approximately 200 s after the onset of membrane shedding (∼1,100 s after initiation of the first division furrow), a focus containing both midbody markers was released into the posterior (P_1) cell (Fig. 1 C, green arrows; Fig. S1 C; and Videos 2 and 3).

Imaging the midbody ring components revealed a similar pattern. As the contractile ring completed its constriction, both Myosin II^{NMY-2}–GFP and GFP–CYK-7 remained concentrated in a tight focus in the center of the cell–cell boundary (Fig. 1 C, yellow arrows; Fig. S1 C; and Video 4). Beginning at anaphase of the second division, tiny fragments of both markers were shed coincident with fragments containing the plasma membrane marker (Fig. 1 C, white arrowheads). When the midbody was released, a large mass of both midbody ring markers was also released from the cell–cell boundary (Figs. 1 C, green arrows; Fig. S1 C; and Video 4). Tracking of the released midbody through the four-cell stage revealed that it was always retained in the EMS cell (Fig. S1 D). Although fragments staining for the plasma membrane marker, which binds phosphatidylinositol 4,5-bisphosphate, were associated with the midbody, the released midbody was not encased in this marker. Thus, the released midbody is either not encased in plasma membrane or the phosphatidylinositol 4,5-bisphosphate associated with the membrane surrounding the midbody is lost during release.

These results suggest that abscission in the early *C. elegans* embryo occurs in two stages (Fig. 2 F). During the first stage, the cytoplasm in the two daughter cells becomes diffusionally isolated, coincident with the completion of furrowing and formation of the intercellular bridge. During the second stage, which begins during anaphase of the subsequent cell division, the cortex surrounding the midbody is remodeled, releasing fragments containing plasma membrane and midbody ring markers. Remodeling culminates, ∼200 s later, in the release of the midbody and midbody ring into the posterior cell.

The ESCRT machinery is required for midbody/midbody ring release

Midbody/midbody ring release could be mediated by ESCRT-dependent membrane scission (Henne et al., 2011; Agromayor and Martin-Serrano, 2013; McCullough et al., 2013). To investigate ESCRT function in the *C. elegans* embryo, we first localized the four-protein ESCRT-I complex by immunofluorescence against $ESCRT\text{-}I^{TSG-101}$ and time-lapse imaging of a GFP fusion with $ESCRT\text{-}I^{MVB-12}$. $ESCRT\text{-}I^{TSG-101}$ colocalized with $MKLP1^{ZEN-4}$ to the midbody at the two-cell stage (Fig. 2 A). GFP–$ESCRT\text{-}I^{MVB-12}$ was first detected at the midbody ∼400 s after furrow initiation; levels subsequently increased (not depicted), and GFP–$ESCRT\text{-}I^{MVB-12}$ was released with other midbody/midbody ring components after anaphase of the second division (Fig. 2 B and Video 5). To analyze ESCRT function, we depleted the ESCRT-I component TSG-101 because of its essential nonredundant role in membrane scission during cytokinesis (Carlton and Martin-Serrano, 2007; Morita et al., 2007). $ESCRT\text{-}I^{TSG-101}$ depletion did not affect the timing of cytoplasmic isolation as assessed by monitoring photoactivated dextran diffusion (Fig. 2 C). During the second stage of abscission, fragments containing the plasma membrane marker and midbody ring markers were shed in *ESCRT-$I^{tsg-101}$(RNAi)* embryos (Fig. 2 E and Fig. S2) with timing similar to that in controls (onset = 9.5 ± 28 s in *ESCRT-$I^{tsg-101}$(RNAi)* embryos [$n = 20$] compared with 24 ± 41 s in control embryos [$n = 66$]). Strikingly, all four midbody/midbody ring components failed to release in the majority of *ESCRT-$I^{tsg-101}$(RNAi)* embryos (Fig. 2, D and E, yellow arrows; Fig. S2; and Video 6) and instead remained at the cell–cell interface even when monitored beyond the four-cell stage (Fig. 2, D and E). Consistent with previous work in *C. elegans* (Audhya et al., 2007; Michelet et al., 2009), furrows were not observed to open back up in ESCRT-inhibited embryos. We conclude that the ESCRT machinery is required to release the midbody/midbody ring from the cell–cell boundary but not for cytoplasmic isolation or to maintain a closed connection between the daughter cells.

$PRC1^{SPD-1}$ depletion prevents the formation of midbody microtubule bundles and Aurora B^{AIR-2} targeting to the intercellular bridge

To examine the role of midbody microtubules in abscission, we depleted the microtubule-bundling protein $PRC1^{SPD-1}$. As in other systems (Mollinari et al., 2002, 2005; Vernì et al., 2004; D'Avino et al., 2007), $PRC1^{SPD-1}$ inhibition in the *C. elegans* embryo prevents the formation of the microtubule bundles that make up the central spindle and blocks midbody assembly (Verbrugghe and White, 2004). We confirmed loss of midbody

of GFP-$ESCRT\text{-}I^{MVB-12}$ before and after release from the cell–cell boundary, respectively. (C) Example of an *ESCRT-$I^{tsg-101}$(RNAi)* embryo in which a 10-kD dextran probe was photoactivated after apparent closure ($n = 4$ embryos). Central plane images show the embryo before activation (−5 s), immediately after activation (5 s), and 140 s after activation (140 s). A kymograph was constructed by aligning strips (narrow rectangle) from images collected at 5-s intervals. Red arrow denotes the point of photoactivation. (D and E, top) Central plane confocal images of *ESCRT-$I^{tsg-101}$(RNAi)* embryos expressing a fluorescently tagged plasma membrane probe along with the midbody marker mCherry-$Mklp1^{ZEN-4}$ (D; $n = 10$ embryos) or the midbody ring marker GFP–CYK-7 (E; $n = 6$ embryos). Times are relative to anaphase of the second division. Released fragments marked with the plasma membrane probe (white arrowheads) and the mCherry-$Mklp1^{ZEN-4}$–marked or GFP–CYK-7–marked midbody remnants are indicated (yellow arrows). Asterisks mark the new midbody/midbody rings arising from the second embryonic division. (bottom) Graphs plotting the times when the mCherry-$Mklp1^{ZEN-4}$–marked midbodies or GFP–CYK-7–marked midbody rings were released in control and *ESCRT-$I^{tsg-101}$(RNAi)* embryos. In cases in which the midbody/midbody ring was not released, the data point reflects the endpoint of the time-lapse sequence. (F) Timeline summarizes the key events during contractile ring constriction (light gray) and abscission (dark gray). MTs, microtubules. White boxes on the low magnification images in A, B, D, and E mark the location of the region shown at higher magnification in the adjacent images. Bars, 5 µm.

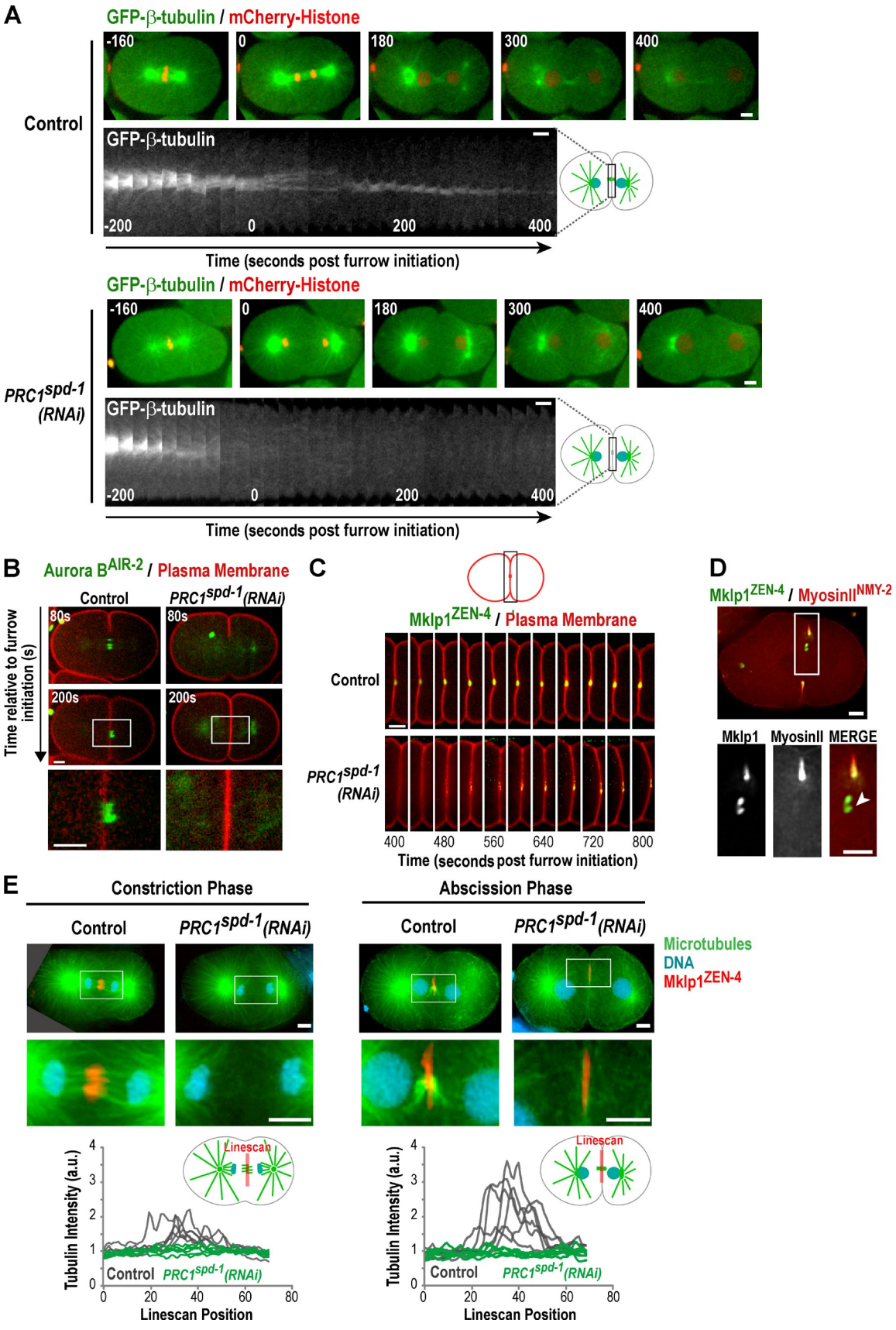

Figure 3. **PRC1^{SPD-1} depletion prevents the formation of midbody microtubule bundles and Aurora B^{AIR-2} targeting to the intercellular bridge.** (A) Central plane confocal images of control (top; *n* = 8 embryos) and *PRC1^{spd-1}(RNAi)* (bottom; *n* = 9) embryos expressing GFP–β-tubulin and mCherry-histone. Kymographs of the GFP–β-tubulin signal in the midbody region are also shown. Times are seconds after furrow initiation. (B) Central plane confocal images

microtubules by imaging control and *PRC1*$^{spd\text{-}1}$*(RNAi)* embryos expressing GFP–β-tubulin and mCherry::histone. In control embryos, bundled microtubules in the central spindle compacted to form the midbody, which could be monitored for >400 s after furrow initiation. After this point, which corresponds to the onset of mitosis of the second cell division, midbody microtubules appeared to dissipate, suggesting that relatively few microtubules span the intracellular bridge at the time of midbody release in control *C. elegans* embryos. In contrast, no central spindle or midbody microtubules were detected at any stage in *PRC1*$^{spd\text{-}1}$*(RNAi)* embryos (Fig. 3 A and Video 7). Consistent with the absence of midbody microtubules, as the furrow closed during the first division, we could not detect any focus of GFP–Aurora B$^{AIR\text{-}2}$ or mCherry-Mklp1$^{ZEN\text{-}4}$ embedded within the cell–cell boundary in *PRC1*$^{spd\text{-}1}$*(RNAi)* embryos (Fig. 3, B and C). Although mCherry-Mklp1$^{ZEN\text{-}4}$ did not localize to the initial cell–cell boundary in *PRC1*$^{spd\text{-}1}$*(RNAi)* embryos, a population of mCherry-Mklp1$^{ZEN\text{-}4}$ was subsequently recruited to the midbody ring, becoming detectable ∼500–600 s after furrow initiation (Fig. 3 C). In control embryos, the amount of mCherry-Mklp1$^{ZEN\text{-}4}$ in the focus at the cell–cell boundary also increased over time (Fig. 3 C). In fixed abscission stage embryos, the freeze-crack fixation procedure occasionally causes the midbody ring to release from the midbody; in such embryos, Mklp1$^{ZEN\text{-}4}$ localized to both the midbody and with Myosin II$^{NMY\text{-}2}$ to the midbody ring (Fig. 3 D). These findings are consistent with work in vertebrate cells, suggesting that Mklp1 transitions from the midbody to the midbody ring as the intercellular bridge matures (Elia et al., 2011; Hu et al., 2012). To further confirm the loss of midbody microtubules in *PRC1*$^{spd\text{-}1}$*(RNAi)* embryos, we performed immunofluorescence in fixed embryos using Mlkp1$^{ZEN\text{-}4}$ as a marker for the location of the midbody ring. Whereas an intense microtubule bundle passed through the Mklp1$^{ZEN\text{-}4}$-marked midbody ring in interphase two-cell stage control embryos, no tubulin fluorescence above background was detected passing through the Mklp1$^{ZEN\text{-}4}$-marked midbody ring in *PRC1*$^{spd\text{-}1}$*(RNAi)* embryos (Fig. 3 E). We conclude that there are no detectable microtubule bundles passing through the intercellular bridge in *PRC1*$^{spd\text{-}1}$*(RNAi)* embryos. Our results further suggest that Mklp1$^{ZEN\text{-}4}$ is a component of the midbody ring as well as the midbody and can be directly recruited to the midbody ring independent of midbody microtubules.

Furrow ingression and cytoplasmic isolation occur with normal timing in the absence of midbody microtubules

Next, we monitored abscission in *PRC1*$^{spd\text{-}1}$*(RNAi)* embryos. The kinetics of contractile ring closure in *PRC1*$^{spd\text{-}1}$*(RNAi)* embryos were similar to those in controls, and apparent closure of the hole between the daughter cells occurred at a similar time point (Fig. 4 A). Monitoring of the contractile/midbody ring components Myosin II$^{NMY\text{-}2}$–GFP, GFP-Septin$^{UNC\text{-}59}$, and GFP–CYK-7 revealed that despite the absence of the midzone/midbody, the contractile ring closed and was converted into a midbody ring embedded in the cell–cell boundary with normal kinetics in *PRC1*$^{spd\text{-}1}$*(RNAi)* embryos (Fig. 4, B and C; and Fig. 5 B).

To determine whether midbody microtubules affect cytoplasmic isolation, we compared the diffusion of photoactivated 10-kD dextran probe at different time points after furrow initiation in control and *PRC1*$^{spd\text{-}1}$*(RNAi)* embryos. To quantitatively compare diffusion across the division plane at different times during furrow ingression, we calculated the normalized intensity difference (NID) between the activated and unactivated halves of the embryo for each time point after photoactivation. Plotting the initial slope of the NID, which reflects the rate of probe diffusion across the division plane (Fig. 3 D), versus time revealed that the rate of diffusion across the division plane decreased with similar kinetics in control and *PRC1*$^{spd\text{-}1}$*(RNAi)* embryos (Fig. 3 E). In both cases, the rate progressively dropped until it reached 0 ∼250 s after furrow initiation; the point at which diffusion stopped was reached slightly sooner (∼30 s) in *PRC1*$^{spd\text{-}1}$*(RNAi)* embryos than in controls. We conclude that midbody microtubules are not required for cytoplasmic isolation.

Midbody microtubules are not required for membrane shedding, ESCRT recruitment, or midbody ring release

Next, we determined whether the absence of midbody microtubules affected membrane shedding or the fate of the midbody ring embedded in the cell–cell boundary. Imaging embryos coexpressing a fluorescent membrane probe with the midbody and midbody ring components revealed that *PRC1*$^{spd\text{-}1}$*(RNAi)* embryos shed fragments containing the plasma membrane marker and midbody ring markers at a time equivalent to that in controls (Fig. 5, A and C; and Video 8). The midbody ring markers Myosin II$^{NMY\text{-}2}$–GFP, GFP-Septin$^{UNC\text{-}59}$, and GFP–CYK-7 were embedded in the cell–cell boundary in the *PRC1*$^{spd\text{-}1}$*(RNAi)* embryos, and this focus was released into the posterior cell with normal timing (Fig. 5, B and C; and Video 8); Mklp1$^{ZEN\text{-}4}$ recruited to the midbody ring was also released into the posterior cell (Fig. S3).

of control (*n* = 5) and *PRC1*$^{spd\text{-}1}$*(RNAi)* (*n* = 5) embryos expressing GFP–Aurora B$^{AIR\text{-}2}$ along with the mCherry-tagged plasma membrane probe. Times are seconds after furrow initiation. (C) The central region of confocal images of control (*n* = 18) and *PRC1*$^{spd\text{-}1}$*(RNAi)* embryos (*n* = 7) expressing a GFP-tagged plasma membrane probe and mCherry-Mklp1$^{ZEN\text{-}4}$ are shown at different time points after furrow initiation. (D) Deconvolved wide-field image (single z plane) of a control embryo stained for Myosin$^{NMY\text{-}2}$ and MKLP1$^{ZEN\text{-}4}$ along with tubulin and DNA (not depicted). DNA condensation and midbody compaction indicate that this is an abscission phase embryo whose furrow retracted during the freeze-crack fixation. Insets show MKLP1$^{ZEN\text{-}4}$ at the midbody (white arrowhead) and overlapping with Myosin$^{NMY\text{-}2}$ on the midbody ring. (E, top) Deconvolved wide-field images of control and *PRC1*$^{spd\text{-}1}$*(RNAi)* embryos fixed during constriction phase (left) or abscission phase (right) and stained for tubulin (green), DNA, and Mklp1$^{ZEN\text{-}4}$. Images are 2-µm projections through the central region of the embryo. (bottom) Traces show line scans (20 × 70 pixels) drawn across the center of control and *PRC1*$^{spd\text{-}1}$*(RNAi)* embryos (*n* = 6 control and 6 *PRC1*$^{spd\text{-}1}$*(RNAi)* embryos for each phase imaged in a single experiment). Intensity values were normalized by dividing by the mean fluorescence intensity in the cytoplasm near the cell periphery. a.u., arbitrary unit. White boxes on the low magnification images in B, D, and E mark the location of the region shown at higher magnification in the images at the bottom. Bars, 5 µm.

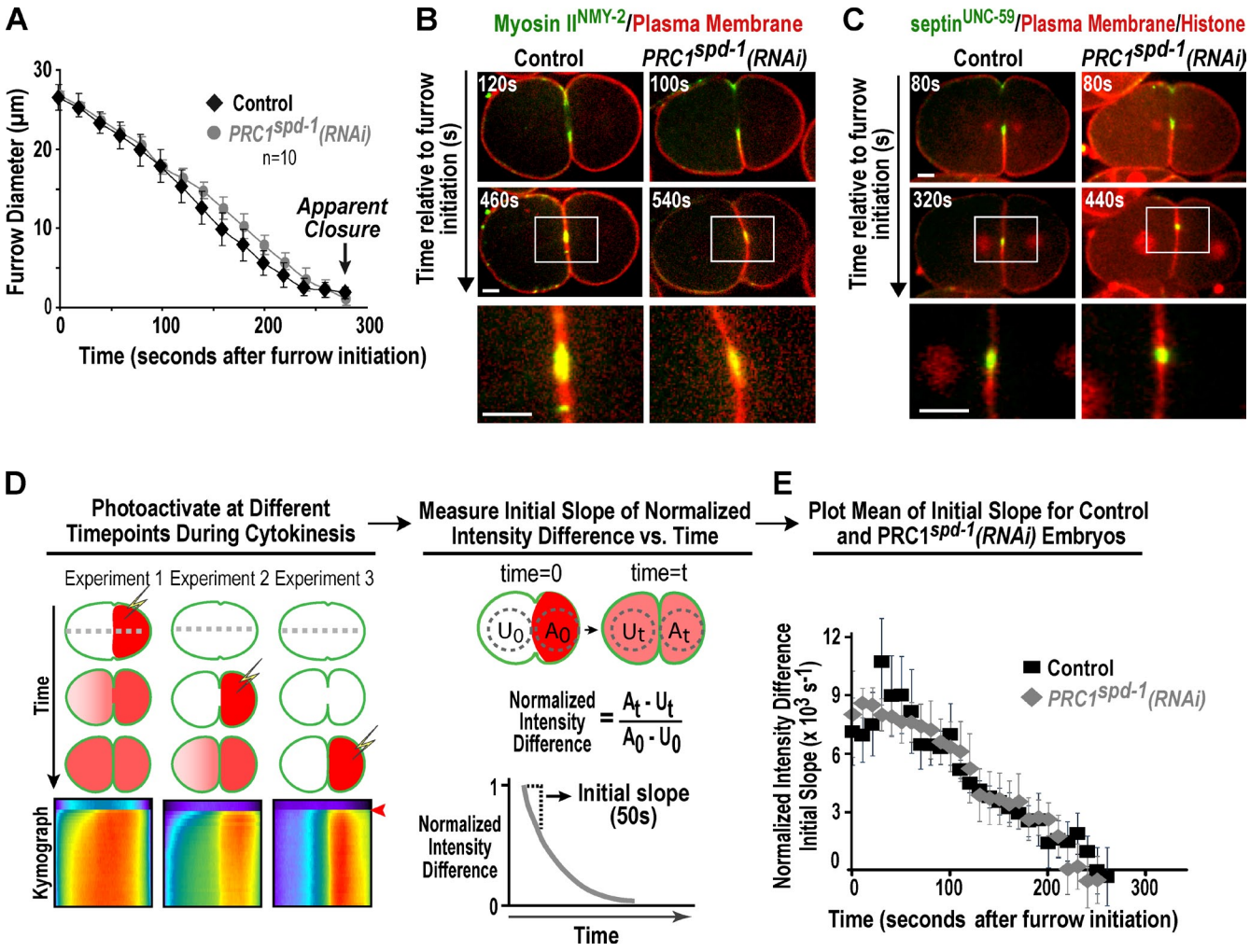

Figure 4. **Furrow ingression and cytoplasmic isolation occur with normal timing in the absence of midbody microtubules.** (A) Graph plotting mean furrow diameter versus time, for the first division of control (reproduced from Fig. 1 A for comparison) and *PRC1*$^{spd\text{-}1}$*(RNAi)* embryos (n = 10 embryos for each condition). Error bars are the SDs. Arrow denotes the last time point with a measurable opening (apparent closure). (B and C) Central plane confocal images of control and *PRC1*$^{spd\text{-}1}$*(RNAi)* embryos expressing Myosin II$^{NMY\text{-}2}$–GFP along with the mCherry-tagged plasma membrane probe (B, n = 5 for each condition) or GFP-septin$^{UNC\text{-}59}$ along with the mCherry-tagged plasma membrane probe and mCherry-histone (C; n = 5 for each condition). Times are seconds after furrow initiation. (D) Outline of the method used to compare cytoplasmic isolation kinetics in control and *PRC1*$^{spd\text{-}1}$*(RNAi)* embryos. Embryos expressing the GFP-tagged plasma membrane probe loaded with 10-kD caged carboxy-Q-rhodamine–labeled dextran were photoactivated on one side at different time points after furrow initiation, and images were collected at 5-s intervals to monitor probe diffusion. Kymographs are shown for embryos photoactivated early in cytokinesis, midcytokinesis, and at closure (the early and closure kymographs are reproduced from Fig. 1 B). Red arrows denote the point of photoactivation. The NID between the activated (A) and unactivated (U) halves of the embryo, calculated as shown, was plotted versus time, and the initial slope of the intensity difference, which reflects the rate of diffusion across the division plane, was calculated. (E) Graph plotting the mean initial slope of the NID versus time in seconds after furrow initiation for control and *PRC1*$^{spd\text{-}1}$*(RNAi)* embryos. Error bars are the 90% confidence interval; mean n = 10 slope measurements per time point. White boxes on the low magnification images in B and C mark the location of the region shown at higher magnification in the images at the bottom. Bars, 5 μm.

The fact that the midbody ring is released normally in *PRC1*$^{spd\text{-}1}$*(RNAi)* embryos suggests that ESCRT can be directly recruited to the midbody ring. Consistent with this expectation, time-lapse imaging revealed recruitment and release of ESCRT-I$^{MVB\text{-}12}$ from the cell–cell boundary (Fig. 4 D). In summary, we conclude that despite the central role proposed for the midbody in orchestrating abscission, all the events we can monitor, including cytoplasmic isolation, ESCRT recruitment, membrane shedding, and release of the midbody ring into the posterior cell, succeed in the absence of midbody microtubules. These findings suggest that the midbody ring may play a greater role in scaffolding abscission than previously appreciated.

The septins are required for timely cytoplasmic isolation and for release of the midbody and midbody ring

The septins are midbody ring components across metazoans and have been shown to be important for abscission in vertebrate and *Drosophila* S2 cells (Estey et al., 2010; Kechad et al., 2012). In contrast to the combinatorial complexity of heterooligomeric septin complexes in humans, which have 13 different septins (Hall and Russell, 2012), *C. elegans* has only two septins (UNC-59 and UNC-61), and depletion of either is sufficient to disrupt septin recruitment to the contractile ring (Nguyen et al., 2000; John et al., 2007). To examine the effects of septin inhibition, we depleted the septin UNC-59. Consistent with

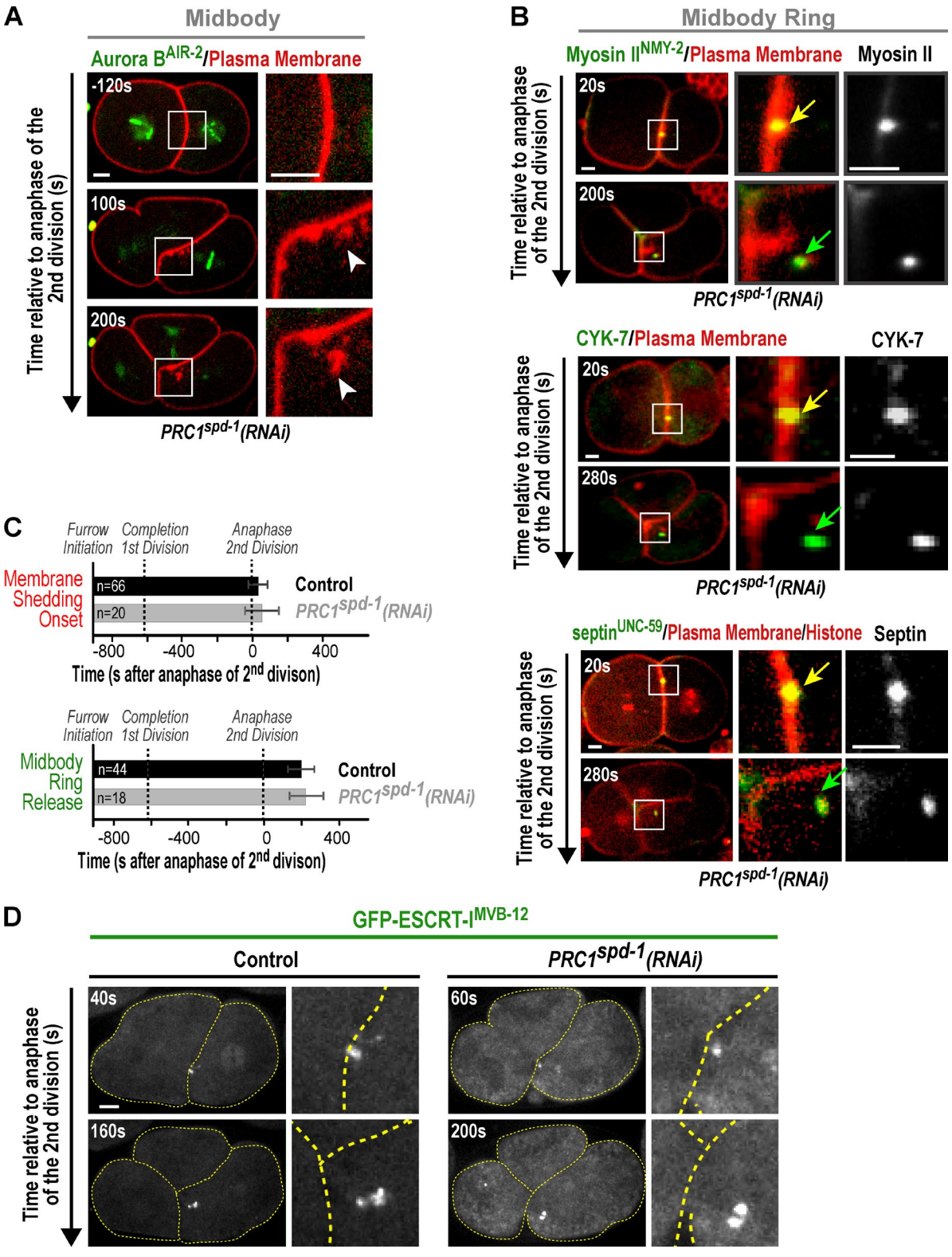

Figure 5. **Midbody microtubules are not required for membrane shedding, ESCRT recruitment, or midbody ring release.** (A) Central plane confocal images showing membrane shedding (white arrowheads) at the cell–cell boundary in a *PRC1*$^{spd\text{-}1}$*(RNAi)* embryo (n = 9 embryos) expressing an mCherry-tagged plasma membrane probe and GFP–Aurora B$^{AIR\text{-}2}$. Times are relative to anaphase of the second division. (B) Central plane confocal images showing midbody ring release in a *PRC1*$^{spd\text{-}1}$*(RNAi)* embryo expressing the midbody ring markers Myosin II$^{NMY\text{-}2}$–GFP (n = 8 embryos), GFP–CYK-7 (n = 10 embryos), or GFP-septin$^{UNC\text{-}59}$ (n = 5 embryos) along with the mCherry-tagged plasma membrane probe and mCherry-histone. Times are relative to anaphase of the second division. Midbody rings are highlighted before (yellow arrows) and after (green arrows) release from the cell–cell junction. (C) Graphs plotting the mean onset of membrane shedding (top) and midbody ring release (bottom) for control and *PRC1*$^{spd\text{-}1}$*(RNAi)* embryos. Error bars are the SDs. (D) Central plane confocal images of control (n = 6 embryos) and *PRC1*$^{spd\text{-}1}$*(RNAi)* (n = 7 embryos) embryos expressing GFP–ESCRT-I$^{MVB\text{-}12}$. Times are relative to anaphase of the second division. Dashed yellow lines mark the cell boundaries. Images are scaled equivalently. White boxes on the low magnification images in A and B mark the location of the region shown at higher magnification in the adjacent images. Bars, 5 µm.

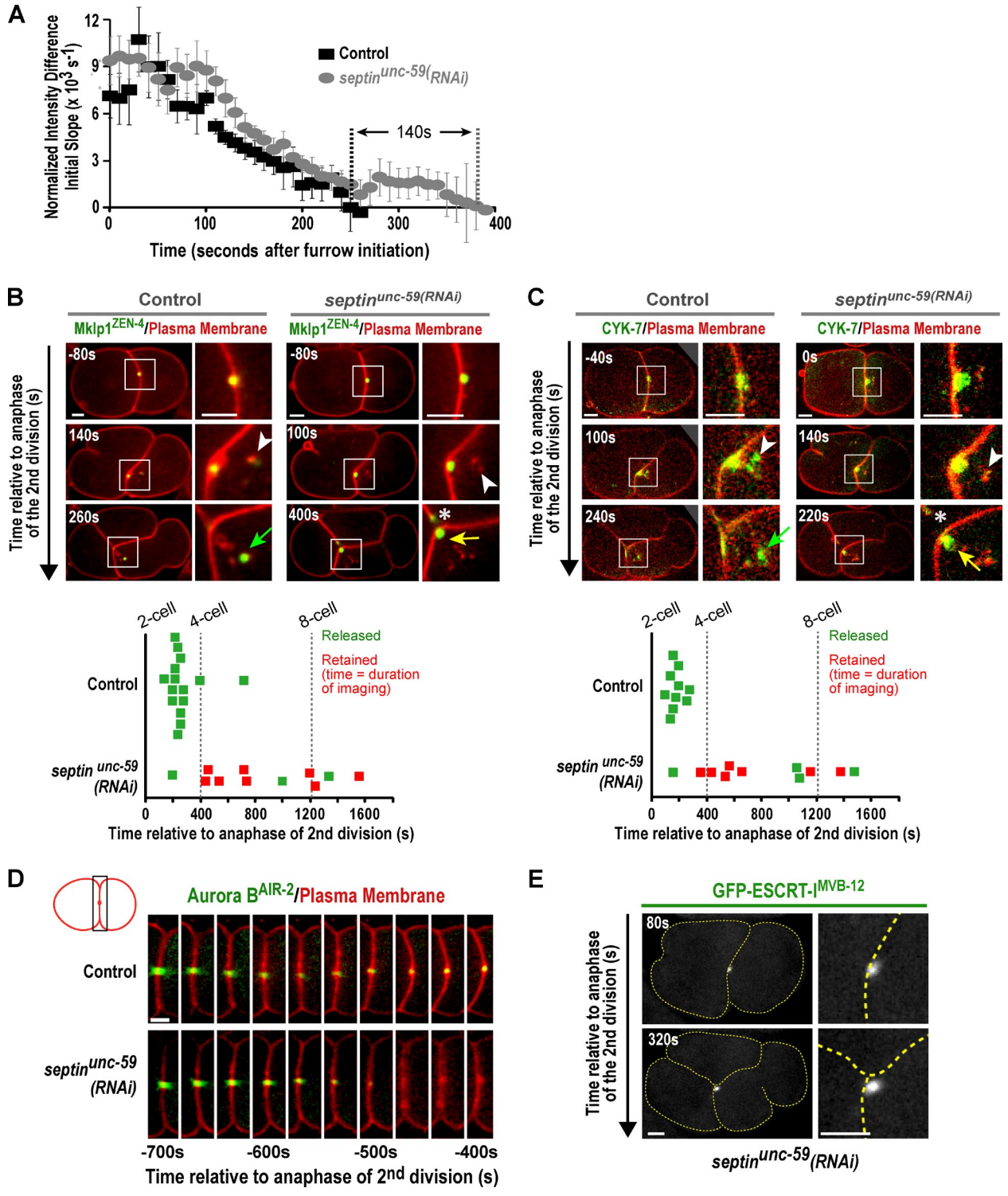

Figure 6. **The septins are required for timely cytoplasmic isolation and for midbody release.** (A) Graph plotting the mean initial slope of the NID versus time in seconds after furrow initiation for control and *septin*$^{unc\text{-}59}$*(RNAi)* embryos. Error bars are the 90% confidence interval; mean $n = 10$ slope measurements per time point. (B and C, top) Central plane confocal images of control and *septin*$^{unc\text{-}59}$*(RNAi)* embryos expressing a fluorescently tagged plasma membrane probe and the midbody markers mCherry-Mklp1$^{ZEN\text{-}4}$ (B; $n = 11$ embryos) or GFP–CYK-7 (C; $n = 11$ embryos). Times are relative to anaphase of the second division. Released fragments marked with the plasma membrane probe are indicated (white arrowheads). Arrows point to the midbody/midbody ring from the first division, which is released in control embryos (green arrows) and fails to be released in *septin*$^{unc\text{-}59}$*(RNAi)* embryos (yellow arrows). Asterisks mark the tip of the ingressing furrow from the second embryonic division. (bottom) Graphs plotting the times when the mCherry-Mklp1$^{ZEN\text{-}4}$–marked midbodies or GFP–CYK-7–marked midbody rings were released. In cases in which the midbody/midbody ring was not released, the data point refers to the endpoint of the time-lapse sequence. (D) The central region of confocal images of control ($n = 11$) and *septin*$^{unc\text{-}59}$*(RNAi)* ($n = 10$) embryos expressing the mCherry-tagged plasma membrane probe and GFP–Aurora B$^{AIR\text{-}2}$. (E) Confocal images of *septin*$^{unc\text{-}59}$*(RNAi)* ($n = 6$ embryos) embryos expressing GFP–ESCRT-I$^{MVB\text{-}12}$. Times in D and E are relative to anaphase of the second division. Dashed yellow lines mark the cell boundaries. Bars, 5 µm.

previous work (Maddox et al., 2007), the furrow closed with similar kinetics to controls until the very end, when *septin$^{unc\text{-}59}$(RNAi)* embryos persisted longer (∼40 s) with a small hole between the daughter cells (Fig. S4 A). To determine how septin depletion affects the timing of cytoplasmic isolation, we used the approach described in Fig. 4 D to monitor the diffusion of photoactivated 10-kD dextran across the division plane. Plotting the mean initial slope of the NID versus time revealed that the rate of diffusion across the division plane decreases with similar kinetics for the first 250 s after furrow initiation. However, at this point, the curves diverge, and the *septin$^{unc\text{-}59}$(RNAi)* embryos remain diffusionally connected, with a small open channel between the daughter cells, for ∼140 s longer than controls (Fig. 6 A). We conclude that cytoplasmic isolation is substantially delayed by septin depletion.

Cytoplasmic isolation normally occurs as the contractile ring envelops the midbody to form the intercellular bridge. The substantial delay in cytoplasmic isolation in the *septin$^{unc\text{-}59}$(RNAi)* embryos suggested that this process was not occurring normally. Consistent with this idea, examination of mCherry-Mklp1$^{ZEN\text{-}4}$ and GFP–CYK-7 revealed that the midbody and midbody ring in *septin$^{unc\text{-}59}$(RNAi)* embryos protruded out toward the cytoplasm in the posterior cell at the two-cell stage (Fig. 6, B and C, top). In contrast to control embryos, in which both mCherry-Mklp1$^{ZEN\text{-}4}$ and GFP–Aurora B$^{AIR\text{-}2}$ remained at the cell–cell junction until midbody release, GFP–Aurora B$^{AIR\text{-}2}$ gradually disappeared from the cell–cell junction in *septin$^{unc\text{-}59}$(RNAi)* two-cell embryos coincident with entry of the daughter cells into mitosis (∼500 s before anaphase of the second division; Fig. 6 D). One possibility, suggested by the fact that midbody microtubules become difficult to detect during this time frame in control embryos, is that Aurora B$^{AIR\text{-}2}$ transitions from midbody microtubules to a septin-dependent localization on the midbody ring coincident with mitotic entry. Shedding of plasma membrane and midbody ring markers was observed in *septin$^{unc\text{-}59}$(RNAi)* embryos coincident with anaphase of the second division (onset = −19 ± 39 s in *septin$^{unc\text{-}59}$(RNAi)* embryos [n = 20] compared with 24 ± 41 s in control embryos [n = 66]). At the time when the midbody and midbody ring were released into the posterior cell in control embryos, a focus containing mCherry–MKLP-1$^{ZEN\text{-}4}$, Myosin II$^{NMY\text{-}2}$–GFP, and GFP–CYK-7 protruded into the posterior cell of *septin$^{unc\text{-}59}$(RNAi)* embryos but did not release (Figs. 6, B and C, yellow arrows; Fig. S4 B; and Video 9). After *septin$^{unc\text{-}59}$(RNAi)*, GFP–ESCRT-I$^{MVB\text{-}12}$ was recruited at levels comparable to controls (Fig. 6 E), but also failed to release, suggesting that the failure to release the midbody/midbody ring in *septin$^{unc\text{-}59}$(RNAi)* embryos was not caused by failure to recruit the ESCRT machinery. We conclude that inhibition of the septins delays cytoplasmic isolation and results in the formation of a defective intercellular bridge; the intercellular bridge permits ESCRT machinery recruitment but cannot support ESCRT-mediated midbody/midbody ring release into the posterior cell.

Septins and ESCRT function at different steps during abscission

Because both ESCRT and septin inhibitions result in failure of midbody/midbody ring release (Fig. 2, D and E; and Fig. 6, B and C), we performed a more careful comparison of these two conditions. In control embryos, expressing a GFP-tagged plasma membrane probe, the ingressing furrow enveloped the midbody, generating a smooth cell–cell boundary. In *septin$^{unc\text{-}59}$(RNAi)* embryos, envelopment of the midbody by the plasma membrane was delayed, but the boundary remained smooth (Fig. 6 A). In *ESCRT-I$^{tsg\text{-}101}$(RNAi)* embryos, the furrow enveloped the midbody with normal timing, consistent with our analysis indicating that cytoplasmic isolation occurs coincident with the completion of furrowing (Fig. 2 C); however, the intercellular bridge was often distended, suggesting the presence of an obstruction enveloped along with the midbody (Fig. 7 A and Video 10). An occlusion was also visible in the cell–cell boundary in differential interference contrast images of *ESCRT-I$^{tsg\text{-}101}$(RNAi)* embryos (Fig. 7 A). Given that we do not observe ESCRT-I on the midbody/midbody ring until after cytoplasmic isolation, we suspect that the obstruction is a consequence of the effect of ESCRT inhibition on the formation of multivesicular bodies (Henne et al., 2011; McCullough et al., 2013), rather than caused by its role in midbody/midbody release. The midbody release defect in septin$^{UNC\text{-}59}$-depleted embryos also differed from that in ESCRT-I$^{TSG\text{-}101}$–depleted embryos. In septin$^{UNC\text{-}59}$-depleted embryos, the midbody/midbody ring protruded into the posterior cell and did not appear to be encased in plasma membrane marker (Fig. 7 B and Fig. 6, B and C). In contrast, in ESCRT-I$^{TSG\text{-}101}$–depleted embryos, the midbody/midbody ring was encased in a ring of plasma membrane embedded in the cell–cell boundary (Fig. 7 B). These distinct defects suggest that the septins and the ESCRT machinery function at different points during abscission (Fig. 8 and accompanying text in the Discussion).

Discussion

Here, we use assays for cytoplasmic diffusion across the division plane and the fate of midbody and midbody ring components to analyze abscission in the early *C. elegans* embryo. Our results partition abscission into two distinct stages and define molecular components required for each stage (Fig. 8). Contrary to the proposal that abscission is orchestrated by the midbody, we show that all events during abscission that we can assay proceed normally in the absence of midbody microtubules. These results suggest that the midbody ring, rather than the midbody, orchestrates abscission in *C. elegans*.

Abscission occurs in two stages: cytoplasmic isolation and midbody/midbody ring release

Previous work in HeLa cells suggested that the cessation of diffusion between the daughter cells and ESCRT-mediated scission are coupled events (Steigemann et al., 2009; Guizetti et al., 2011). In contrast, our characterization partitions abscission into two temporally distinct stages with different molecular requirements. During the first stage (Fig. 8, early abscission), the cytoplasm in the daughter cells becomes diffusionally isolated, coincident with the formation of an intercellular bridge containing the midbody and midbody ring. This step requires the septins but is ESCRT independent. During the second stage

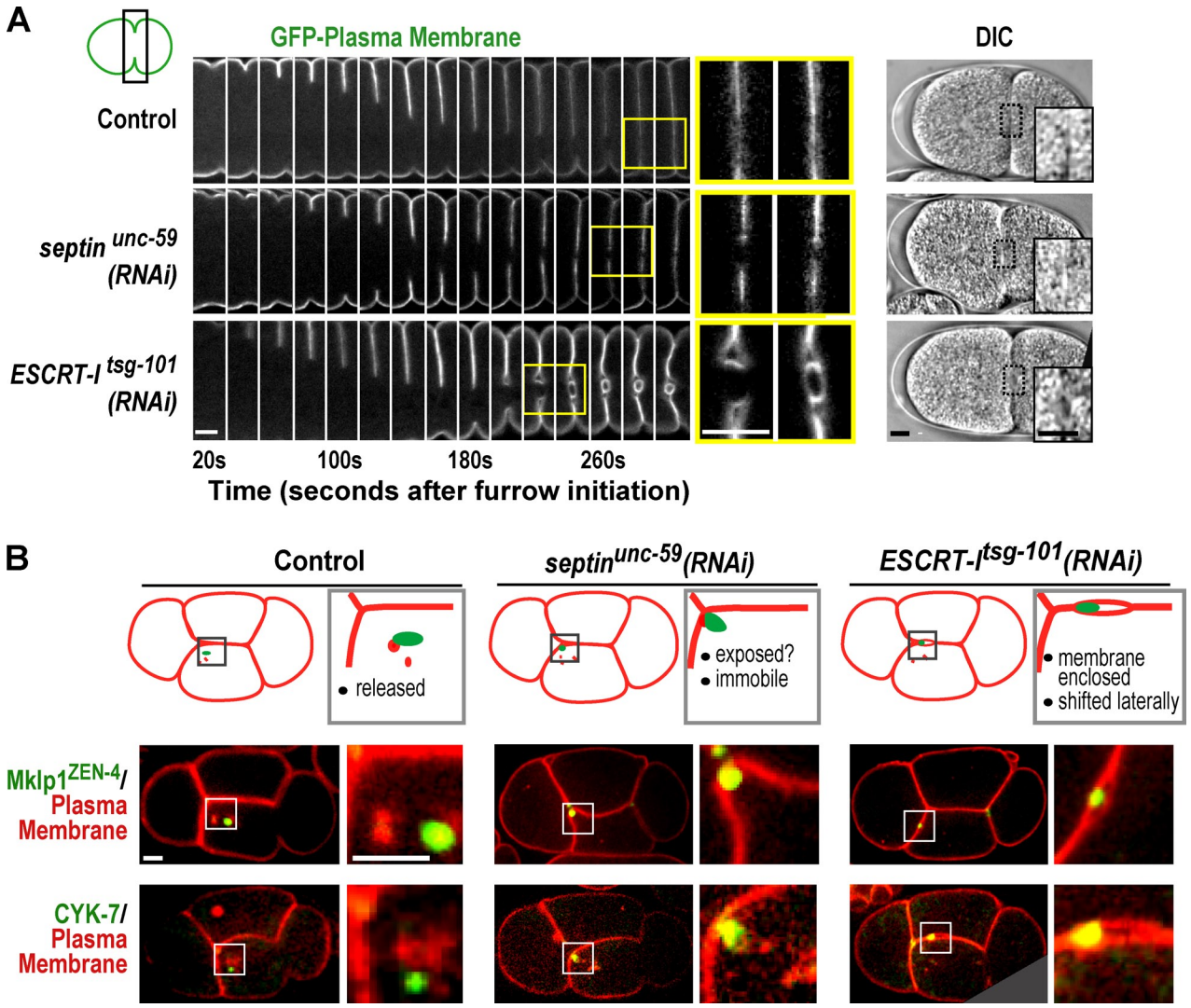

Figure 7. **The septins and ESCRT machinery function at different stages of abscission.** (A, left) The central region of confocal images of control, *septin*$^{unc-59}$*(RNAi)*, and *ESCRT-I*$^{tsg-101}$*(RNAi)* (>10 embryos for each condition) embryos expressing a GFP-tagged plasma membrane probe at different time points after furrow initiation. (right) Differential interference contrast (DIC) images of control, *septin*$^{unc-59}$*(RNAi)*, or *ESCRT-I*$^{tsg-101}$*(RNAi)* embryos at the two-cell stage. The region in the yellow boxes is shown at higher magnification in the images to the right. (B) Central plane confocal images of four-cell stage control, *septin*$^{unc-59}$*(RNAi)*, and *ESCRT-I*$^{tsg-101}$*(RNAi)* embryos expressing a fluorescently tagged plasma membrane probe along with the midbody marker mCherry-MKLP1^{ZEN-4} (top; *n* = 21 control, 12 *septin*$^{unc-59}$*(RNAi)*, and 16 *ESCRT-I*$^{tsg-101}$*(RNAi)* embryos) or the midbody ring marker GFP–CYK-7 (bottom; *n* = 19 control, 12 *septin*$^{unc-59}$*(RNAi)*, and 6 *ESCRT-I*$^{tsg-101}$*(RNAi)* embryos). The midbody is released into the posterior cell in control embryos, protrudes from cell–cell boundary in *septin*$^{unc-59}$*(RNAi)* embryos, and is enclosed within a plasma membrane–bound compartment embedded in the cell–cell boundary in *ESCRT-I*$^{tsg-101}$*(RNAi)* embryos. White boxes on the low magnification images mark the location of the region shown at higher magnification in the adjacent images. Bars, 5 µm.

(Fig. 8, late abscission), which occurs concurrent with the subsequent division of the daughter cells, the intercellular bridge is remodeled, as indicated by plasma membrane shedding, followed by the ESCRT-dependent release of the midbody/midbody ring. Remodeling of the intercellular bridge releases fragments containing plasma membrane and midbody ring markers (Fig. 8, late abscission–membrane shedding). Membrane shedding is observed after septin^{UNC-59}, PRC1^{SPD-1}, and ESCRT-I$^{TSG-101}$ depletion. An attractive possibility based on these results is that shedding is the result of a septin- and ESCRT-independent membrane remodeling event that acts on the intercellular bridge in conjunction with the ESCRT machinery to release the midbody/midbody ring. Additional work targeting some of the membrane trafficking components implicated in abscission (Schiel and Prekeris, 2013) will be needed to determine how membrane shedding occurs and to assess its importance to abscission.

Our results show that the septins are required for release of the midbody/midbody ring as well as for timely cytoplasmic isolation. In septin-inhibited embryos, cytoplasmic isolation eventually occurs, but the midbody/midbody ring ends up in an aberrant configuration protruding into the posterior cell (Fig. 8). Thus, when the septins are absent, a septin-independent process is able to bring about cytoplasmic isolation, albeit in an aberrant way that does not result in the midbody/midbody ring being properly enveloped within the cell–cell boundary. In septin-depleted embryos, the ESCRT machinery is recruited, but the midbody/midbody ring fails to release. An appealing possibility is that release fails because

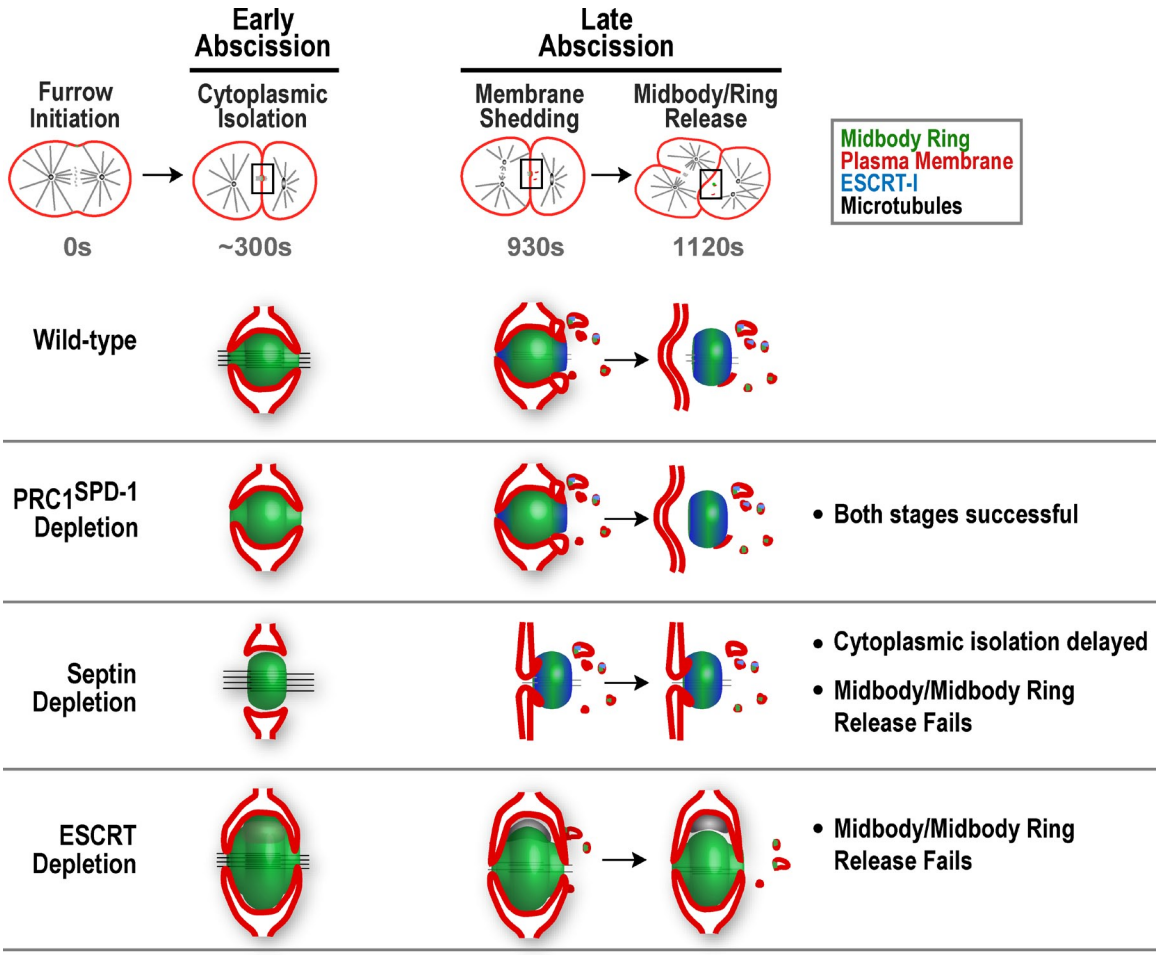

Figure 8. **Model for the roles of midbody microtubules, the septins, and the ESCRT machinery in the two stages of abscission in the *C. elegans* embryo.** Abscission occurs in two stages in wild-type *C. elegans* embryos. In the first stage (early abscission), cytoplasmic isolation occurs as furrow ingression completes, and an intercellular bridge forms between the two daughter cells (~300 s). The second stage (late abscission) occurs almost one cell cycle later, coincident with the onset of anaphase of the second round of cell division. During late abscission, the intercellular bridge is remodeled, releasing fragments containing plasma membrane and cortical components (membrane shedding; 930 s), and the midbody and midbody ring are released into the posterior cell via an ESCRT-dependent process (midbody/ring release; 1,120 s). In PRC1^{SPD-1}-depleted embryos, events during both early and late abscission occur with normal kinetics. In septin-depleted embryos, events during both early and late abscission are defective, cytoplasmic isolation is delayed, and the midbody and midbody ring fail to release into the posterior cell. When the ESCRT machinery is depleted, the furrow envelops the midbody, and cytoplasmic isolation occurs with normal timing. However, the intercellular bridge is distended, suggesting the presence of an occlusion enveloped along with the midbody. As the intercellular bridge matures, the midbody and midbody ring are pushed to one side of the intercellular bridge and fail to release into the posterior cell.

the aberrant cell–cell junction that forms is unable to serve as a substrate for the ESCRT-mediated scission machinery.

In the *C. elegans* embryo, the midbody/midbody ring is released one cell cycle after the intercellular bridge is formed. We do not know what mechanical or cell cycle cues control the timing of midbody release. Although cell cycle regulation seems to be the most likely trigger, recent work in human cells has shown that a local reduction in tension promotes abscission in vertebrate cells (Lafaurie-Janvore et al., 2013). It will therefore be interesting to determine whether midbody release in *C. elegans* is controlled by cell cycle cues or by an alteration in cortical tension induced by cell shape changes at anaphase of the second division.

The midbody ring orchestrates abscission in the absence of midbody microtubules

A central focus of our work was to test the hypothesis that the microtubule-based midbody serves as the platform that brings together the abscission machinery. Remarkably, all of the events that we monitored during both stages of abscission, cytoplasmic isolation, shedding of membrane and midbody ring components, and midbody/midbody ring release, all succeeded when we prevented midbody assembly by inhibiting the microtubule-bundling protein PRC1^{SPD-1}. This result suggests that the midbody is not an essential component of the diffusion barrier between daughter cells; the midbody ring can close the hole between the daughter cells sufficiently to block cytoplasmic diffusion.

Midbody microtubules are also proposed to scaffold the recruitment of membrane trafficking components that narrow the intercellular bridge before scission (Schiel and Prekeris, 2013) and of the ESCRT machinery to promote scission (Fededa and Gerlich, 2012; Agromayor and Martin-Serrano, 2013). Our results suggest that the midbody ring, in the absence of midbody microtubules, is sufficient to direct remodeling of the intercellular

bridge to allow it to attain a conformation conducive to cleavage and to recruit the ESCRT machinery that releases the midbody/midbody ring. Previous work in HeLa cells showed that PRC1^{SPD-1} depletion results in an abscission defect (Mollinari et al., 2005). These authors reported that furrowing proceeded to completion, and cells remained connected by an intercellular bridge for ∼1 h, the usual time between formation of the intercellular bridge and scission (Steigemann et al., 2009; Guizetti et al., 2011) before the furrow regressed. These results suggest that the defect in these cells might not be in the formation of the intercellular bridge but in the execution of the final scission event (Mollinari et al., 2005). Additional work using higher resolution assays for the different steps in abscission will be needed to determine which step in abscission is blocked in the absence of PRC1 and whether remodeling of the intercellular bridge in human cells is affected by the absence of midbody microtubules.

In human cells, centralspindlin recruits CEP55, which recruits the ESCRT machinery to promote scission (Fabbro et al., 2005; Zhao et al., 2006; Carlton and Martin-Serrano, 2007; Morita et al., 2007; Carlton et al., 2008; Lee et al., 2008; Bastos and Barr, 2010). Because *C. elegans* (and *Drosophila*) lack CEP55 homologues, the ESCRT machinery is likely recruited in these systems either by direct binding to centralspindlin or another midbody ring component. Direct binding to centralspindlin is an attractive possibility, as centralspindlin is recruited directly to the midbody ring with similar timing to the ESCRT complex in PRC1^{SPD-1}-depleted embryos (Fig. 3 C). As centralspindlin also transitions from the midbody to the midbody ring in human cells (Elia et al., 2011; Hu et al., 2012), it is possible that centralspindlin and the ESCRT machinery are recruited to the abscission site in human cells lacking midbody microtubules, as they are in *C. elegans*, but that scission fails as a result of a role for midbody microtubules downstream of ESCRT recruitment. Additional experiments will be needed to resolve this issue.

Abscission phase in vivo

Our work provides a detailed molecular analysis of abscission in an organismal context. One of our most interesting findings is how robust abscission is in the *C. elegans* embryo. Cell–cell boundaries form and remain stably closed in cells lacking midbody microtubules, depleted of the ESCRT machinery, and depleted of the septins, all conditions previously shown to result in abscission failure and reopening of the intercellular bridge in vertebrate cells (Mollinari et al., 2005; Estey et al., 2010; Caballe and Martin-Serrano, 2011). Consistent with this finding, cell–cell boundaries have previously been shown to form and remain closed, even in the presence of chromatin obstructions (Bembenek et al., 2013). The fact that we did not see regression of cell–cell boundaries under any of the conditions we tested suggests that redundant mechanisms are in place to ensure the successful formation of stable cell–cell boundaries in intact organisms. The nature of these mechanisms will be an interesting area to explore in future work.

Materials and methods

C. elegans strains

C. elegans strains (genotypes listed in Table S1) were maintained at 20°C. As the *gfp::air-2* transgene in OD448 is subject to silencing, experiments with this line were performed by singling adult OD448 hermaphrodites after confirming that they were positive for the GFP::AIR-2 marker and using L4 progeny from these animals for experiments. GFP::AIR-2 expression was verified in the pronuclei of dissected embryos before midbody filming.

RNAi

Double-stranded RNAs (dsRNAs) were prepared by using oligonucleotides (oligos) containing T3 or T7 promoters (listed in Table S2) to amplify regions from genomic N2 DNA. PCR reactions were cleaned (QIAGEN) and used as templates for T3 and T7 transcription reactions (25 µl; Ambion), which were cleaned using a MEGAclear kit (Ambion) and combined. RNA eluted with 50 µl H_2O was mixed with 3× injection buffer (25 µl; 1× = 20 mM KPO_4, pH 7.5, 3 mM K-Citrate, pH 7.5, and 2% PEG 6000) and annealed by incubating at 68°C for 10 min followed by 37°C for 30 min. dsRNA was injected into L4 hermaphrodite worms 48 h before imaging. For photoactivation experiments, the gonads of dsRNA-injected worms were reinjected with CMNCBZ-caged carboxy-Q-rhodamine dextran (Invitrogen and Molecular Probes) 43 h later (5 h before imaging).

Photoactivation experiments

Adult OD58 (Audhya et al., 2005) hermaphrodites, either injected 43 h previously with dsRNA or uninjected controls, were injected in both gonads with a 10,000 molecular weight dextran conjugate of CMNCBZ-caged carboxy-Q-rhodamine dissolved in injection buffer (20 mM KPO_4, pH 7.5, 3 mM K-Citrate, pH 7.5, and 2% PEG 6000) at a concentration of 5 mg/ml. Worms were discarded if injections spilled into the body cavity because this resulted in embryos containing aggregated probe, presumably caused by endocytic uptake of the probe into oocytes. Worms were allowed to recover at 20°C for 5 h on plates with food. We note that *ESCRT-I$^{tsg-101}$(RNAi)* adversely affected cuticle formation in the adult worm, making reinjection more difficult than for the other depletion conditions; shortened, more rigid needles were used to inject these worms. Dissected embryos were mounted for filming by transferring selected embryos to a preformed 2% agarose pad positioned on microscope slide with a mouth pipette and covering them with an 18 × 18–mm coverslip. Photoactivation and imaging of dissected embryos were performed on a deconvolution microscope (DeltaVision; Applied Precision) equipped with a charge-coupled device (CCD) camera (CoolSNAP; Roper Scientific). Mounted embryos were positioned so that half of the embryo was blocked from light exposure when the field diaphragm was closed completely. Prephotoactivation images were taken with the field diaphragm open (at 5-s intervals). Then, the field diaphragm was manually closed, and the embryo was hit with a 2-s pulse of UV light using a 100-W mercury arc lamp (Chiu Technical Corporation) to uncage the probe and produce orange fluorescence (excitation/emission of ∼545/575 nm). The field diaphragm was reopened, and a single central z section was acquired at 5-s intervals for 100 s using a 60×, NA 1.4 Plan Apochromat objective (Olympus) with 2 × 2 binning.

Images were analyzed in MetaMorph (Molecular Devices) by positioning two 90-pixel diameter circles on either side of the furrow site (activated versus unactivated sides) and logging the total intensity in the rhodamine channel over the time series. The total value for each side before photoactivation (background) was subtracted from the total value at each time interval after photoactivation to eliminate baseline rhodamine signal. The NID (NID = $[A_t - U_t]/[A_0 - U_0]$) was calculated for each time point, at which $A_t - U_t$ was the difference between the fluorescence intensities of the activated and unactivated sides at time t, and $A_0 - U_0$ was the difference between the fluorescence intensities of the activated and unactivated sides at the first time point after activation. The initial slope of the NID (−d/dt NID), which reflects the rate of diffusion across the division plane, was calculated for the 50-s interval after photoactivation as follows ($NID_{t=50} - NID_{t=0}$)/50 s. By shifting the analysis window, each photoactivation event was used to estimate six initial slopes at 10-s intervals spanning the 100 s after photoactivation. Individual embryos were often photoactivated two times (i.e., once before furrow initiation and then once at the end of closure). For the control plot (Fig. 4 E and Fig. 6 A), data from 55 independent photoactivations in 42 embryos were pooled, yielding a mean of 11.7 measured slopes per 10-s interval. For the *PRC1^{spd-1}(RNAi)* plot (Fig. 4 E), data from 47 independent photoactivations in 37 embryos were pooled, yielding a mean of 10.6 measured slopes per 10-s interval. For the *septin^{unc-59}(RNAi)* plot (Fig. 6 A), data from 61 independent photoactivations in 33 embryos were pooled yielding a mean of 9.9 measured slopes per 10-s interval. To generate the graphs in Fig. 4 E and Fig. 6 A, the slope data from all of the photoactivation events were pooled, and the mean value of the slope for each 10-s interval centered on the plotted point was calculated.

Plots of furrow diameter versus time

Plots of furrow diameter versus time (Fig. 1 A, Fig. 4 A, and Fig. S4 A) were generated by collecting 12-plane z series (2.5-µm intervals) at 20-s time intervals of embryos from the strain OD58 during the course of the first embryonic division on a deconvolution microscope (DeltaVision) equipped with a CCD camera (CoolSNAP). DeltaVision software was used to rotate the data from the central region of the embryo containing the contractile ring by 90° and generate a maximum intensity projection and to measure the diameter of the hole at each time point.

Midbody/midbody ring release experiments

One-cell stage embryos were dissected from gravid adult hermaphrodites from the strains OD449, OD183, OD1268, OD448, OD178, OD868, and OD297 in M9 medium (Brenner, 1974) and were mounted for imaging by transferring them to a 2% agarose pad with a mouth pipette and covering them with a 18 × 18–mm coverslip. Images were acquired with either (a) an confocal system (Revolution XD; Andor Technology) with a confocal scanner unit (CSU-10; Yokogawa Corporation of America) mounted on an inverted microscope (TE2000-E; Nikon) equipped with a 60×, 1.4 NA Plan Apochromat lens, solid-state 100-mW lasers, and a high-resolution interline CCD camera (Clara [Andor Technology; 2 × 2 binning] or iXon [Andor Technology; 1 × 1 binning]) or (b) a microscope (Axio Observer.Z1; Carl Zeiss) equipped with a CCD camera (ORCA-ER; Hamamatsu Photonics) with 2 × 2 binning. Embryos were imaged every 20 s in a single image plane, manually adjusting to keep the midbody in focus, until ∼800 s after furrow initiation. To track the dynamics of the midbody before and at midbody release, an 8 × 1–µm z series was then collected every 20 s until the embryo reached the four-cell stage. Single planes containing the midbody remnant were identified and stitched together to generate movies using MetaMorph software. Live imaging of microtubules (Fig. 3 A) was performed by acquiring a central eight-plane z series (1-µm steps) at 20-s time intervals throughout the first and second division; a single image plane, containing microtubules, at each time point was selected and stitched together to track changes at the midbody. Timing of membrane shedding onset and midbody/midbody ring release was gauged relative to (a) furrow initiation, which we define as the first dimpling of the plasma membrane, or (b) anaphase of the second division in the anterior (AB) cell, which was scored on the basis of the distinct round to squarelike shape change in the plasma membrane boundary.

Immunofluorescence

Immunofluorescence was performed by dissecting 5–10 worms with a scalpel in a 2.2-µl drop of water onto a slide coated with 1 mg/ml poly-L-lysine (P-1524; Sigma-Aldrich). Coated slides were dried on a hot plate and baked for 30 min in a 100°C oven before use. Dissected worms were covered with a 10-mm square coverslip, and the slide was immersed in liquid nitrogen. Slides were removed from the nitrogen, and coverslips were flicked off; slides were immediately plunged into −20°C methanol bath. After 20 min, the slides were rehydrated in PBS (2 × 5 min). The edges of the slide were dried with a Kimwipe (Kimberly-Clark), avoiding the region with the adhered embryos, which was circled with a PAP pen. Embryos were blocked by pipetting on 50 µl AbDil (PBS, 4% BSA, and 0.1% Triton X-100) for 20 min before incubation with 1 µg/ml antibodies directed against TSG-101 (Audhya et al., 2007), NMY-2 (Maddox et al., 2005), ANI-1 (Anillin; Maddox et al., 2005), or ZEN-4 (Lewellyn et al., 2010) that were directly labeled with either Cy3 or Cy5 (CyDye Monoreactive Dye Packs; GE Healthcare) according to manufacturer's instructions. Microtubules were labeled by either performing the immunofluorescence in embryos expressing GFP::TBA-2 (Fig. 2 A) or by probing with FITC-labeled α-tubulin antibodies (1:500 DM1-α; Abcam; Fig. 3 E). Slides were washed 3× with PBST (PBS + 0.1% Triton X-100) and once with PBST + 1 µg/ml Hoechst and then mounted in 4 µl PPD (0.5% *p*-phenylenediamine, 20 mM Tris-Cl, pH 8.8, and 90% glycerol) under an 18 × 18–mm coverslip. Coverslips were sealed with nail polish. Images in Fig. 3 E were acquired using a 100×, 1.35 NA U-Plan Apochromat oil objective lens (Olympus) mounted on a DeltaVision system that included a microscope (IX70; Olympus) equipped with a camera (CoolSNAP CCD). Images in Fig. 2 A were acquired on a swept field confocal microscope (Ti-E; Nikon) equipped with a CCD camera (CoolSNAP HQ2) using a Nikon 60×, 1.4 NA Plan Apochromat oil objective lens. Acquisition parameters were controlled by Elements software (Nikon). For embryo immunofluorescence, ∼100 z sections at 0.2-µm steps were acquired, three-dimensional datasets were computationally deconvolved using softWoRx software (Applied Precision), and relevant sections were used to generate maximum intensity projections. Line scans (20 × 70 pixels; Fig. 3 E) were drawn across the embryo center, and mean intensity values for each pixel position were recorded using MetaMorph software. Pixel intensities were normalized by dividing by the mean fluorescence intensity in the cytoplasm near the cell periphery (mean of the first and last 10 pixel values along the trace) before plotting intensity versus line scan position.

Online supplemental material

Fig. S1, related to Fig. 1, illustrates loading of embryos with dextran, GFP–Aurora $B^{AIR\text{-}2}$, and GFP–CYK-*7* in control embryos and that the first division midbody/midbody ring ends up in the EMS cell. Fig. S2, related to Fig. 2, shows GFP–Aurora $B^{AIR\text{-}2}$ and Myosin $II^{NMY\text{-}2}$–GFP in *ESCRT-I$^{tsg\text{-}101}$(RNAi)* embryos. Fig. S3, related to Fig. 5, shows release of $MKLP1^{ZEN\text{-}4}$ in control and *PRC1$^{spd\text{-}1}$(RNAi)* embryos. Fig. S4 shows furrow diameter versus time in *septin$^{unc\text{-}59}$(RNAi)* embryos, Myosin $II^{NMY\text{-}2}$–GFP in *septin$^{unc\text{-}59}$(RNAi)* embryos, and persistent diffusion of photoactivated probe in a *septin$^{unc\text{-}59}$(RNAi)* embryo. Table S1 shows *C. elegans* strains used in this study. Table S2 shows oligos used for dsRNA production. Video 1, related to Fig. 1 B, shows dextran photoactivation before cytokinesis onset and after apparent closure. Videos 2, 3, and 4, related to Fig. 1, show $Mklp1^{ZEN\text{-}4}$ (Video 2), Aurora $B^{AIR\text{-}2}$ (Video 3), CYK-*7* (Video 4), and Myosin $II^{NMY\text{-}2}$ (Video 4) during abscission. Video 5, related to Fig. 2, shows GFP–ESCRT-$I^{MVB\text{-}12}$ during abscission. Video 6, related to Fig. 2, shows Aurora $B^{AIR\text{-}2}$ and CYK-*7* in *ESCRT-I$^{tsg\text{-}101}$(RNAi)* embryos. Video 7, related to Fig. 3, shows chromosomes and spindle microtubules in control and *PRC1$^{spd\text{-}1}$(RNAi)* embryos. Video 8, related to Fig. 5, shows Aurora $B^{AIR\text{-}2}$ and CYK-*7* in *PRC1$^{spd\text{-}1}$(RNAi)* embryos. Video 9, related to Fig. 6, shows $Mklp1^{ZEN\text{-}4}$ and CYK-*7* in *septin$^{unc\text{-}59}$(RNAi)* embryos. Video 10, related to Fig. 7, shows that ESCRT-$I^{TSG\text{-}101}$ depletion leads to a distended intercellular bridge. Online supplemental material is available at http://www.jcb.org/cgi/content/full/jcb.201306036/DC1.

We thank members of the Oegema and Desai laboratories for helpful suggestions.

R. Green was supported by a fellowship from the American Cancer Society (PF-06-254-01-CCG). K. Oegema and A. Desai receive salary and additional support from the Ludwig Institute for Cancer Research. J. Audhya is funded by National Institutes of Health (GM088151).

Submitted: 7 June 2013
Accepted: 9 October 2013

References

Agromayor, M., and J. Martin-Serrano. 2013. Knowing when to cut and run: mechanisms that control cytokinetic abscission. *Trends Cell Biol.* 23:433–441. http://dx.doi.org/10.1016/j.tcb.2013.04.006

Audhya, A., F. Hyndman, I.X. McLeod, A.S. Maddox, J.R. Yates III, A. Desai, and K. Oegema. 2005. A complex containing the Sm protein CAR-1 and the RNA helicase CGH-1 is required for embryonic cytokinesis in *Caenorhabditis elegans*. *J. Cell Biol.* 171:267–279. http://dx.doi.org/10.1083/jcb.200506124

Audhya, A., I.X. McLeod, J.R. Yates, and K. Oegema. 2007. MVB-12, a fourth subunit of metazoan ESCRT-I, functions in receptor downregulation. *PLoS ONE.* 2:e956. http://dx.doi.org/10.1371/journal.pone.0000956

Bastos, R.N., and F.A. Barr. 2010. Plk1 negatively regulates Cep55 recruitment to the midbody to ensure orderly abscission. *J. Cell Biol.* 191:751–760. http://dx.doi.org/10.1083/jcb.201008108

Bembenek, J.N., K.J. Verbrugghe, J. Khanikar, G. Csankovszki, and R.C. Chan. 2013. Condensin and the spindle midzone prevent cytokinesis failure induced by chromatin bridges in *C. elegans* embryos. *Curr. Biol.* 23:937–946. http://dx.doi.org/10.1016/j.cub.2013.04.028

Brenner, S. 1974. The genetics of *Caenorhabditis elegans*. *Genetics*. 77:71–94.

Caballe, A., and J. Martin-Serrano. 2011. ESCRT machinery and cytokinesis: the road to daughter cell separation. *Traffic*. 12:1318–1326. http://dx.doi.org/10.1111/j.1600-0854.2011.01244.x

Carlton, J.G., and J. Martin-Serrano. 2007. Parallels between cytokinesis and retroviral budding: a role for the ESCRT machinery. *Science*. 316:1908–1912. http://dx.doi.org/10.1126/science.1143422

Carlton, J.G., M. Agromayor, and J. Martin-Serrano. 2008. Differential requirements for Alix and ESCRT-III in cytokinesis and HIV-1 release. *Proc. Natl. Acad. Sci. USA*. 105:10541–10546. http://dx.doi.org/10.1073/pnas.0802008105

Carmena, M., M. Wheelock, H. Funabiki, and W.C. Earnshaw. 2012. The chromosomal passenger complex (CPC): from easy rider to the godfather of mitosis. *Nat. Rev. Mol. Cell Biol.* 13:789–803. http://dx.doi.org/10.1038/nrm3474

Chai, Y., D. Tian, Y. Yang, G. Feng, Z. Cheng, W. Li, and G. Ou. 2012. Apoptotic regulators promote cytokinetic midbody degradation in *C. elegans*. *J. Cell Biol.* 199:1047–1055. http://dx.doi.org/10.1083/jcb.201209050

Chen, C.-T., A.W. Ettinger, W.B. Huttner, and S.J. Doxsey. 2013. Resurrecting remnants: the lives of post-mitotic midbodies. *Trends Cell Biol.* 23:118–128. http://dx.doi.org/10.1016/j.tcb.2012.10.012

D'Avino, P.P. 2009. How to scaffold the contractile ring for a safe cytokinesis - lessons from Anillin-related proteins. *J. Cell Sci.* 122:1071–1079. http://dx.doi.org/10.1242/jcs.034785

D'Avino, P.P., V. Archambault, M.R. Przewloka, W. Zhang, K.S. Lilley, E. Laue, and D.M. Glover. 2007. Recruitment of Polo kinase to the spindle midzone during cytokinesis requires the Feo/Klp3A complex. *PLoS ONE*. 2:e572. http://dx.doi.org/10.1371/journal.pone.0000572

Elia, N., R. Sougrat, T.A. Spurlin, J.H. Hurley, and J. Lippincott-Schwartz. 2011. Dynamics of endosomal sorting complex required for transport (ESCRT) machinery during cytokinesis and its role in abscission. *Proc. Natl. Acad. Sci. USA*. 108:4846–4851. http://dx.doi.org/10.1073/pnas.1102714108

Estey, M.P., C. Di Ciano-Oliveira, C.D. Froese, M.T. Bejide, and W.S. Trimble. 2010. Distinct roles of septins in cytokinesis: SEPT9 mediates midbody abscission. *J. Cell Biol.* 191:741–749. http://dx.doi.org/10.1083/jcb.201006031

Fabbro, M., B.-B. Zhou, M. Takahashi, B. Sarcevic, P. Lal, M.E. Graham, B.G. Gabrielli, P.J. Robinson, E.A. Nigg, Y. Ono, and K.K. Khanna. 2005. Cdk1/Erk2- and Plk1-dependent phosphorylation of a centrosome protein, Cep55, is required for its recruitment to midbody and cytokinesis. *Dev. Cell*. 9:477–488. http://dx.doi.org/10.1016/j.devcel.2005.09.003

Fededa, J.P., and D.W. Gerlich. 2012. Molecular control of animal cell cytokinesis. *Nat. Cell Biol.* 14:440–447. http://dx.doi.org/10.1038/ncb2482

Gai, M., P. Camera, A. Dema, F. Bianchi, G. Berto, E. Scarpa, G. Germena, and F. Di Cunto. 2011. Citron kinase controls abscission through RhoA and anillin. *Mol. Biol. Cell*. 22:3768–3778. http://dx.doi.org/10.1091/mbc.E10-12-0952

Glotzer, M. 2009. The 3Ms of central spindle assembly: microtubules, motors and MAPs. *Nat. Rev. Mol. Cell Biol.* 10:9–20. http://dx.doi.org/10.1038/nrm2609

Green, R.A., H.-L. Kao, A. Audhya, S. Arur, J.R. Mayers, H.N. Fridolfsson, M. Schulman, S. Schloissnig, S. Niessen, K. Laband, et al. 2011. A high-resolution *C. elegans* essential gene network based on phenotypic profiling of a complex tissue. *Cell*. 145:470–482. http://dx.doi.org/10.1016/j.cell.2011.03.037

Green, R.A., E. Paluch, and K. Oegema. 2012. Cytokinesis in animal cells. *Annu. Rev. Cell Dev. Biol.* 28:29–58. http://dx.doi.org/10.1146/annurev-cellbio-101011-155718

Guizetti, J., L. Schermelleh, J. Mäntler, S. Maar, I. Poser, H. Leonhardt, T. Müller-Reichert, and D.W. Gerlich. 2011. Cortical constriction during abscission involves helices of ESCRT-III-dependent filaments. *Science*. 331:1616–1620. http://dx.doi.org/10.1126/science.1201847

Hall, P.A., and S.E.H. Russell. 2012. Mammalian septins: dynamic heteromers with roles in cellular morphogenesis and compartmentalization. *J. Pathol.* 226:287–299. http://dx.doi.org/10.1002/path.3024

Henne, W.M., N.J. Buchkovich, and S.D. Emr. 2011. The ESCRT pathway. *Dev. Cell*. 21:77–91. http://dx.doi.org/10.1016/j.devcel.2011.05.015

Hu, C.-K., M. Coughlin, and T.J. Mitchison. 2012. Midbody assembly and its regulation during cytokinesis. *Mol. Biol. Cell*. 23:1024–1034. http://dx.doi.org/10.1091/mbc.E11-08-0721

Hyman, A.A. 1989. Centrosome movement in the early divisions of *Caenorhabditis elegans*: a cortical site determining centrosome position. *J. Cell Biol.* 109:1185–1193. http://dx.doi.org/10.1083/jcb.109.3.1185

John, C.M., R.K. Hite, C.S. Weirich, D.J. Fitzgerald, H. Jawhari, M. Faty, D. Schläpfer, R. Kroschewski, F.K. Winkler, T. Walz, et al. 2007. The *Caenorhabditis elegans* septin complex is nonpolar. *EMBO J.* 26:3296–3307. http://dx.doi.org/10.1038/sj.emboj.7601775

Keating, H.H., and J.G. White. 1998. Centrosome dynamics in early embryos of *Caenorhabditis elegans. J. Cell Sci.* 111:3027–3033.

Kechad, A., S. Jananji, Y. Ruella, and G.R.X. Hickson. 2012. Anillin acts as a bifunctional linker coordinating midbody ring biogenesis during cytokinesis. *Curr. Biol.* 22:197–203. http://dx.doi.org/10.1016/j.cub.2011.11.062

Lafaurie-Janvore, J., P. Maiuri, I. Wang, M. Pinot, J.-B. Manneville, T. Betz, M. Balland, and M. Piel. 2013. ESCRT-III assembly and cytokinetic abscission are induced by tension release in the intercellular bridge. *Science*. 339:1625–1629. http://dx.doi.org/10.1126/science.1233866

Lee, H.H., N. Elia, R. Ghirlando, J. Lippincott-Schwartz, and J.H. Hurley. 2008. Midbody targeting of the ESCRT machinery by a noncanonical coiled coil in CEP55. *Science*. 322:576–580. http://dx.doi.org/10.1126/science.1162042

Lekomtsev, S., K.-C. Su, V.E. Pye, K. Blight, S. Sundaramoorthy, T. Takaki, L.M. Collinson, P. Cherepanov, N. Divecha, and M. Petronczki. 2012. Centralspindlin links the mitotic spindle to the plasma membrane during cytokinesis. *Nature*. 492:276–279. http://dx.doi.org/10.1038/nature11773

Lewellyn, L., J. Dumont, A. Desai, and K. Oegema. 2010. Analyzing the effects of delaying aster separation on furrow formation during cytokinesis in the *Caenorhabditis elegans* embryo. *Mol. Biol. Cell*. 21:50–62. http://dx.doi.org/10.1091/mbc.E09-01-0089

Lo, C.W., and N.B. Gilula. 1979. Gap junctional communication in the preimplantation mouse embryo. *Cell*. 18:399–409. http://dx.doi.org/10.1016/0092-8674(79)90059-X

Madaule, P., M. Eda, N. Watanabe, K. Fujisawa, T. Matsuoka, H. Bito, T. Ishizaki, and S. Narumiya. 1998. Role of citron kinase as a target of the small GTPase Rho in cytokinesis. *Nature*. 394:491–494. http://dx.doi.org/10.1038/28873

Maddox, A.S., B. Habermann, A. Desai, and K. Oegema. 2005. Distinct roles for two *C. elegans* anillins in the gonad and early embryo. *Development*. 132:2837–2848. http://dx.doi.org/10.1242/dev.01828

Maddox, A.S., L. Lewellyn, A. Desai, and K. Oegema. 2007. Anillin and the septins promote asymmetric ingression of the cytokinetic furrow. *Dev. Cell*. 12:827–835. http://dx.doi.org/10.1016/j.devcel.2007.02.018

McCullough, J., L.A. Colf, and W.I. Sundquist. 2013. Membrane fission reactions of the mammalian ESCRT pathway. *Annu. Rev. Biochem.* 82:663–692. http://dx.doi.org/10.1146/annurev-biochem-072909-101058

Michelet, X., A. Alberti, L. Benkemoun, N. Roudier, C. Lefebvre, and R. Legouis. 2009. The ESCRT-III protein CeVPS-32 is enriched in domains distinct from CeVPS-27 and CeVPS-23 at the endosomal membrane of epithelial cells. *Biol. Cell*. 101:599–615. http://dx.doi.org/10.1042/BC20090025

Mollinari, C., J.-P. Kleman, W. Jiang, G. Schoehn, T. Hunter, and R.L. Margolis. 2002. PRC1 is a microtubule binding and bundling protein essential to maintain the mitotic spindle midzone. *J. Cell Biol.* 157:1175–1186. http://dx.doi.org/10.1083/jcb.200111052

Mollinari, C., J.-P. Kleman, Y. Saoudi, S.A. Jablonski, J. Perard, T.J. Yen, and R.L. Margolis. 2005. Ablation of PRC1 by small interfering RNA demonstrates that cytokinetic abscission requires a central spindle bundle in mammalian cells, whereas completion of furrowing does not. *Mol. Biol. Cell*. 16:1043–1055. http://dx.doi.org/10.1091/mbc.E04-04-0346

Morita, E., V. Sandrin, H.-Y. Chung, S.G. Morham, S.P. Gygi, C.K. Rodesch, and W.I. Sundquist. 2007. Human ESCRT and ALIX proteins interact with proteins of the midbody and function in cytokinesis. *EMBO J.* 26:4215–4227. http://dx.doi.org/10.1038/sj.emboj.7601850

Mostowy, S., and P. Cossart. 2012. Septins: the fourth component of the cytoskeleton. *Nat. Rev. Mol. Cell Biol.* 13:183–194.

Nguyen, T.Q., H. Sawa, H. Okano, and J.G. White. 2000. The *C. elegans* septin genes, unc-59 and unc-61, are required for normal postembryonic cytokineses and morphogenesis but have no essential function in embryogenesis. *J. Cell Sci.* 113:3825–3837.

Oh, Y., and E. Bi. 2011. Septin structure and function in yeast and beyond. *Trends Cell Biol.* 21:141–148. http://dx.doi.org/10.1016/j.tcb.2010.11.006

Piekny, A.J., and A.S. Maddox. 2010. The myriad roles of Anillin during cytokinesis. *Semin. Cell Dev. Biol.* 21:881–891. http://dx.doi.org/10.1016/j.semcdb.2010.08.002

Sanger, J.M., M.B. Pochapin, and J.W. Sanger. 1985. Midbody sealing after cytokinesis in embryos of the sea urchin *Arabacia punctulata. Cell Tissue Res.* 240:287–292. http://dx.doi.org/10.1007/BF00222337

Schiel, J.A., and R. Prekeris. 2013. Membrane dynamics during cytokinesis. *Curr. Opin. Cell Biol.* 25:92–98. http://dx.doi.org/10.1016/j.ceb.2012.10.012

Steigemann, P., C. Wurzenberger, M.H.A. Schmitz, M. Held, J. Guizetti, S. Maar, and D.W. Gerlich. 2009. Aurora B-mediated abscission checkpoint protects against tetraploidization. *Cell*. 136:473–484. http://dx.doi.org/10.1016/j.cell.2008.12.020

Verbrugghe, K.J.C., and J.G. White. 2004. SPD-1 is required for the formation of the spindle midzone but is not essential for the completion of cytokinesis in *C. elegans* embryos. *Curr. Biol.* 14:1755–1760. http://dx.doi.org/10.1016/j.cub.2004.09.055

Vernì, F., M.P. Somma, K.C. Gunsalus, S. Bonaccorsi, G. Belloni, M.L. Goldberg, and M. Gatti. 2004. Feo, the *Drosophila* homolog of PRC1, is required for central-spindle formation and cytokinesis. *Curr. Biol.* 14:1569–1575. http://dx.doi.org/10.1016/j.cub.2004.08.054

Waddle, J.A., J.A. Cooper, and R.H. Waterston. 1994. Transient localized accumulation of actin in *Caenorhabditis elegans* blastomeres with oriented asymmetric divisions. *Development*. 120:2317–2328.

Walczak, C.E., and S.L. Shaw. 2010. A MAP for bundling microtubules. *Cell*. 142:364–367. http://dx.doi.org/10.1016/j.cell.2010.07.023

White, E.A., and M. Glotzer. 2012. Centralspindlin: at the heart of cytokinesis. *Cytoskeleton (Hoboken)*. 69:882–892. http://dx.doi.org/10.1002/cm.21065

Zhao, W.-M., A. Seki, and G. Fang. 2006. Cep55, a microtubule-bundling protein, associates with centralspindlin to control the midbody integrity and cell abscission during cytokinesis. *Mol. Biol. Cell*. 17:3881–3896. http://dx.doi.org/10.1091/mbc.E06-01-0015